A Deep Dynamic Latent Block Model for the Co-clustering of Zero-Inflated Data Matrices

Giulia Marchello, Marco Corneli, Charles Bouveyron

A Deep Dynamic Latent Block Model for Co-clustering of Zero-Inflated Data Matrices

Giulia Marchello
Université Côte d'Azur, Inria, CNRS, Laboratoire J.A.Dieudonné,
Maasai team, Nice, France.
and
Marco Corneli
Université Côte d'Azur, Laboratoire CEPAM, Nice, France.
and
Charles Bouveyron
Université Côte d'Azur, Inria, CNRS, Laboratoire J.A.Dieudonné,
Maasai team, Nice, France.

January 22, 2025

Abstract

The simultaneous clustering of observations and features of data sets (known as co-clustering) has recently emerged as a central machine learning application to summarize massive data sets. However, most existing models focus on continuous and dense data in stationary scenarios, where cluster assignments do not evolve over time. This work introduces a novel latent block model for the dynamic co-clustering of data matrices with high sparsity. To properly model this type of data, we assume that the observations follow a time and block dependent mixture of zero-inflated distributions, thus combining stochastic processes with the time-varying sparsity modeling. To detect abrupt changes in the dynamics of both cluster memberships and data sparsity, the mixing and sparsity proportions are modeled through systems of ordinary differential equations. The inference relies on an original variational procedure whose maximization step trains fully connected neural networks in order to solve the dynamical systems. Numerical experiments on simulated and real world data sets demonstrate the effectiveness of the proposed methodology in the context of count data.

Keywords: Co-clustering, Latent Block Model, zero-inflated distributions, dynamic systems, VEM algorithm.

1 Introduction

1.1 Context

Along with the exponential increase in the availability of data in different domains, machine learning techniques that can summarize them using clustering techniques, for example, are also increasing. For instance, large social networking and online shopping platforms are eager to simultaneously clustering users and products to offer the best recommendations to their customers. Similarly, for pharmacovigilance, being an activity of monitoring adverse drug reaction (ADRs), it is very important to create consistent clusters of drugs and ADRs in order to be able to check for atypical phenomena in the development of claims. However, it often happens that classical clustering methods are not efficient in identifying homogeneous and interpretable groups when dealing with data sets containing a high number of variables (i.e. in high dimension for structured data, Lu et al., 2023). Co-clustering is particularly useful in the context of high dimensional data since it simultaneously clusters the rows (observations) and the columns (features) of a data matrix, thus providing useful summaries of the data (Gallaugher et al., 2022). Moreover, in a wide range of applications such as recommending systems,(Liang et al., 2021), biomedical data (Robert, 2017), finance (Fenn et al., 2012), there is an increasing need to develop machine learning models to treat time-dependent data matrices. Although the study in this field has been greatly expanded by many notable methods introduced in the last few decades, the development of dynamic co-clustering methods still remains almost an unexplored territory.

1.2 Related Work

Related work in this context can be split into two main points.

Co-clustering and Latent Block Models Simultaneous clusters of observations and features can be of great help while analyzing a given data set. Co-clustering methods can be distinguished into metric based approaches, such as non-negative matrix trifactorization (NMTF, Labiod and Nadif, 2011; Ding et al., 2006), spectral co-clustering

(Dhillon, 2001), information theory (Dhillon et al., 2003), maximum entropy approach (Banerjee et al., 2007), and model-based co-clustering approaches (e.g. Bouveyron et al., 2019). Among those approaches, model-based co-clustering is widely appreciated for its sound statistical foundations and its flexibility in terms of sparsity and data types. The cornerstone of model-based co-clustering is the popular latent block model (LBM) (Govaert and Nadif, 2003) that was initially introduced for the co-clustering of binary data matrices. LBM is based on the assumption that rows and columns are grouped in hidden clusters and that observations within a block (intersection of a row cluster and a column cluster) are independent and identically distributed. Whereas the original formulation of the model dealt with binary data only, the model has been extended in the last two decades to count data (Govaert and Nadif, 2010), continuous data (Lomet, 2012), categorical data (Keribin et al., 2015), ordinal data (Jacques and Biernacki, 2018; Corneli et al., 2020), functional data (Bouveyron et al., 2018), textual data (Bergé et al., 2019) and mixed-type data (Selosse et al., 2020). Recently, Boutalbi et al. (2020) also proposed the tensor latent block model (TLBM) for co-clustering, whose aim is to simultaneously cluster rows and columns of a 3D matrix, where covariates represent the third dimension. TLBM was also implemented for different types of data sets: continuous data (Gaussian TLBM), binary data (Bernoulli TLBM) and contingency tables (Poisson TLBM).

Dynamic models for clustering and co-clustering Whereas there is a decade-long literature about static model-based clustering and co-clustering methods, dynamic models are more recent in this context. It is worth noting that much more work has been made in the context of network clustering. In particular, for the Stochastic Block Model (SBM, Nowicki and Snijders, 2001) than for LBM, although SBM is a special case of LBM, not needing that data matrices are square and/or symmetrical. Yang et al. (2011) proposed a dynamic version of SBM by allowing the cluster of each node to switch at time $t + 1$ depending on its current state at time t, in a Markovian framework, where the switching probabilities are collected into a transition matrix. In a more general framework, Matias and Miele (2017) showed that, in dynamic SBMs, it is not possible to let vary over time both

the connectivity parameters and cluster memberships without incurring into identifiability issues. Recently, Marchello et al. (2022) proposed an extension of LBM allowing one to perform the simultaneous clustering of rows, columns and slices of a three dimensional counting tensor. Although being a first attempt to extend LBM to the dynamic case, this model has the limitation of not allowing cluster switches of rows/columns. In a different framework, Casa et al. (2021) extended the latent block model to deal with longitudinal data, relying on the shape invariant model (Lindstrom, 1995) and Boutalbi et al. (2021) developed a model-based co-clustering method for sparse three-way data, where the third dimension can be seen as a discrete temporal one. Here, the sparsity is handled following the same assumption as in Ailem et al. (2017) that all blocks outside the main diagonal share the same parameter.

However, these methods, while a first step toward the dynamic expansion of co-clustering methods, can be used mostly for macroscopic analysis, as they do not allow for the temporal dependence of variables.

1.3 Contribution of this work

In this paper, we introduce a co-clustering method to deal with time evolving data matrices, potentially very sparse. In order to model the evolving generating process that gives the data and simultaneously accounts for the data sparsity, we assume that the observations follow a time and block dependent mixture of zero-inflated distributions. Since we co-cluster the row and columns of the data matrices, we introduce two evolving latent random variables that model the group memberships of observations and features, respectively. Moreover, the parameters of the random variables and the data sparsity proportion arise from three systems of ordinary differential equations that model the dynamics. Capturing the data dynamics is crucial in order to detect atypical phenomena that affected the generative process. For instance, if at a given time t_0 the value of some features suddenly increases for just one observation in a group, that observation will be very likely switched to another cluster, from t_0 on, when fitting our model to the data. This example suggests an interpretation of the results which is quite intuitive: a change in the affiliation

of the observations/features to the clusters means that a change point has been detected, leaving space for further analysis to inspect the causes. Thus, we develop a highly interpretable co-clustering method allowing practitioners to obtain a faster visualization of the results in order to automate the data analysis. The proposed model can be used both as a tool for retrospective analysis, but also, and above all, as a tool for near real-time and analysis of the data progression. The code is publicly available on GitHub on the link: `https://github.com/giuliamar95/Zip-dLBM` and in the Supplementary Materials.

1.4 Organization of the paper

This paper is organized as follows. Section 2 first recalls the original latent block model, before introducing the proposed generative model. In Section 3, the inference procedure is detailed. Section 4 presents various experiments on simulated data to test and evaluate the model performances. In Section 5, an application to a real world data set is presented. The London Bike sharing data set is analyzed in order to illustrate the potential of the proposed model. Section 6 provides some concluding remarks.

2 A Zero-Inflated dynamic LBM

In this section, we first recall the standard latent block model, then we introduce the Zero-Inflated Dynamic Latent Block model (Zero-Inflated dLBM).

Notation. The observed data are assumed to be collected into time evolving matrices, over the interval $[0, T]$. We work in discrete time[1] and assume that we have a time partition of equally spaced points

$$0 = t_0 < t_1 < t_u \leq t_U = T.$$

Now up to rescaling, we can assume without loss of generality, that $t_{u+1} - t_u = 1$. Moreover, to simplify the exposition we omit the subscript u and, with a slight abuse of notation, we

[1]This assumption is needed to make the inference tractable. As such, we could describe the generative model in continuous time and move to discrete time in Section 3. However, in order to keep the exposition as simple as possible, we decided to introduce this assumption now.

denote by t the generic time point t_u and by T the number of time points U. Thus, at (discretized) time t, we introduce the incidence matrix $X(t) \in \mathbb{N}^{N \times M}$ whose entry $X_{i,j}(t)$ represents its generic element and it contains the observations and features that took place between t and $t-1$. The rows of $X(t)$ are indexed by $i = 1, ..., N$ and the columns by $j = 1, ..., M$.

2.1 The latent block model

Let us first recall the LBM model which considers a single data matrix. Assuming that the time period is restricted to one time point, the data is a $N \times M$ random matrix $X = \{X_{ij}\}_{i \in 1,...,N, j \in 1,...,M}$. In the LBM framework, rows and columns of X are assumed to be clustered respectively into Q and L groups, such that the data belonging to the same block are independent and identically distributed. More formally, the latent structure of rows and columns of X is identified by the following latent variables:

- $Z := \{z_{iq}\}_{i \in 1,...,N, q \in 1,...,Q}$ represents the clustering of rows into Q groups. Hence, row i belongs to cluster q if $z_{iq} = 1$;
- $W := \{w_{j\ell}\}_{j \in 1,...,M, \ell \in 1,...,L}$ represents the clustering of columns into L groups. Hence, column j belongs to cluster ℓ if $w_{j\ell} = 1$.

Moreover, Z and W are assumed to be independent and distributed according to multinomial distributions:

$$p(Z|\alpha) = \prod_{i=1}^{N} \prod_{q=1}^{Q} \alpha_q^{z_{iq}}, \qquad p(W|\beta) = \prod_{j=1}^{M} \prod_{\ell=1}^{L} \beta_\ell^{w_{j\ell}},$$

where $\alpha_q = \mathbb{P}\{z_{iq} = 1\}$, $\beta_\ell = \mathbb{P}\{w_{j\ell} = 1\}$, $\sum_{q=1}^{Q} \alpha_q = 1$ and $\sum_{\ell=1}^{L} \beta_\ell = 1$. LBM further assumes that, conditionally to Z and W, the entries X_{ij} are independent and their distribution $\varphi(\cdot; \zeta)$ belongs to the same parametric family:

$$X_{ij} \mid z_{iq} w_{j\ell} = 1 \sim \varphi(X_{ij}; \zeta_{q\ell}),$$

where ζ denotes the parameter set of the distribution $\varphi(X_{ij}, \cdot)$, which only depends on the given block. With these assumptions, the complete data likelihood can be written as:

$$p(X, Z, W \mid \alpha, \beta, \zeta) = p(Z \mid \alpha)p(W \mid \beta)p(X|Z, W, \zeta) = \\ = \prod_{i=1}^{N}\prod_{q=1}^{Q} \alpha_q^{z_{iq}} \prod_{j=1}^{M}\prod_{\ell=1}^{L} \beta_\ell^{w_{j\ell}} \prod_{i,q}\prod_{j,\ell} \varphi(X_{ij}; \zeta_{q\ell})^{z_{iq}w_{j\ell}}.$$

Here, we define $\alpha = (\alpha_1, \ldots, \alpha_Q)$, $\beta = (\beta_1, \ldots, \beta_L)$, and the parameter set ζ, whose generic element is $\zeta_{q\ell}$.

2.2 A Zero-Inflated Dynamic Latent Block Model

We now aim at simultaneously clustering the rows and columns of the collection of data matrices $\{X(t)\}_t$ evolving along the time.

2.2.1 Clusters modeling

The rows (i.e. observations) and columns (i.e. features) of $X(t)$ are clustered into Q and L groups, respectively. Although Q and L are assumed fixed over time, each row/column is nevertheless allowed to change cluster membership, in $[0, T]$. More formally, the cluster memberships of the rows and columns of X are identified by two evolving multinomial distributions, respectively parameterized by $\alpha(t)$ and $\beta(t)$:

$$Z_i(t) \overset{iid}{\sim} \mathcal{M}(1, \alpha(t) := (\alpha_1(t), \ldots, \alpha_Q(t))),$$

where $Z_i(t)$ is the i-th row of $Z(t)$, $\mathcal{M}(1, \cdot)$ denotes the multinomial probability mass function and $\alpha_q(t) = \mathbb{P}\{z_{iq}(t) = 1\}$, with $\sum_{q=1}^{Q} \alpha_q(t) = 1$, at time $t = 0, \ldots, T$.
Thus $Z(t) := \{z_{iq}(t)\}_{i\in 1,\ldots,N; q\in 1,\ldots,Q}$ represents the clustering of N rows into Q groups at a given time point t. In a similar fashion, for the column clusters, we assume:

$$W_j(t) \overset{iid}{\sim} \mathcal{M}(1, \beta(t) := (\beta_1(t), \ldots, \beta_L(t))),$$

where $W_j(t)$ is the j-th row of $W(t)$, $\beta_\ell(t) = \mathbb{P}\{w_{j\ell}(t) = 1\}$ and $\sum_{\ell=1}^{L} \beta_\ell(t) = 1$.
The two random arrays Z and W are further assumed to be independent.

2.2.2 Sparsity Modeling

In order to model a potential extreme sparsity, the observed data are assumed to be modeled by a mixture of block-conditional Zero-Inflated (ZI) distributions, where the entries $X_{ij}(t)$ are conditionally independent[2]:

$$X_{ij}(t)|Z_i(t), W_j(t) \sim ZI(\zeta_{Z_i(t),W_j(t)}; \pi(t)) \ , \tag{1}$$

where ζ is a $Q \times L$ denotes the block-dependent parameter set of the distribution $\varphi(X_{ij}(t), \cdot)$, and $\pi(t)$ is a vector of length T that indicates the level of sparsity at any given time period. Being a mixture between a chosen distribution and a Dirac mass at zero, the Zero-Inflated distribution is used to account for a high sparsity in the data and can be formally written as:

$$\begin{cases} X_{ij}(t)|Z_i(t), W_j(t) \sim \delta_0(X_{ij}(t)) & \text{with probability } \pi(t) \\ X_{ij}(t)|Z_i(t), W_j(t) \sim \varphi(X_{ij}(t); \zeta_{Z_i(t);W_j(t)}) & \text{with probability } 1 - \pi(t). \end{cases} \tag{2}$$

where $\delta_0(\cdot)$ is the Dirac function in 0.

Then, to model time-evolving sparsity, we rewrite Eq. (2) by introducing a hidden random matrix, $A \in \{0, 1\}^{N \times M}$, where:

$$A_{ij}(t) \sim \mathcal{B}(\pi(t)),$$

with $\mathcal{B}(p)$ denoting the Bernoulli probability mass function of parameter p and such that

$$\begin{aligned} A_{ij}(t) = 1 &\Rightarrow X_{ij}(t)|Z_i(t), W_j(t) \sim \delta_0(X_{ij}(t)) \\ A_{ij}(t) = 0 &\Rightarrow X_{ij}(t)|Z_i(t), W_j(t) \sim \varphi(X_{ij}(t); \zeta_{Z_i(t),W_j(t)}). \end{aligned} \tag{3}$$

Among the possible distribution of $\varphi(\cdot)$, one of the most widely used is the Poisson distribution (ZIP (Zero-Inflated Poisson), Lambert, 1992) for count data, or the log-normal and the Gamma distributions for continuous data.

[2]When no confusion arises we adopt in Eq. (1) a quite common convention in the clustering literature: $Z_i(t)$ denotes both the i-th row of $Z(t)$ and a random variable whose value is q if row i is in the q-th row cluster at time t; the same convention stands for for $W_j(t)$.

2.2.3 Modeling the temporal evolution of the parameters

The last assumption concerns the modeling of clusters proportions and sparsity over time. In fact, the mixing parameters $\alpha(t)$ and $\beta(t)$ as well as the sparsity proportions $\pi(t)$ are assumed to be driven by a system of ordinary differential equations (ODEs). In this way, we are able to capture the temporal evolution of both the clusters composition and the (excess of) sparsity. In continuous time, the three dynamic systems reads as:

$$\frac{d}{dt}a(t) = f_Z(a(t)), \qquad \frac{d}{dt}b(t) = f_W(b(t)), \qquad \frac{d}{dt}c(t) = f_A(c(t)), \tag{4}$$

where $t \in [0, T]$, $f_Z : \mathbb{R}^Q \to \mathbb{R}^Q$, $f_W : \mathbb{R}^L \to \mathbb{R}^L$ and $f_A : \mathbb{R} \to \mathbb{R}$ are three unknown continuous functions $a : [0, T] \to \mathbb{R}^Q$, $b : [0, T] \to \mathbb{R}^L$ and $c : [0, T] \to \mathbb{R}$ are three continuously differentiable functions such that

$$\alpha_q(t) = \text{softmax}(a_q(t)) = \frac{e^{a_q(t)}}{\sum_{q=1}^{Q} e_q^a(t)},$$

$$\beta_\ell(t) = \text{softmax}(b_\ell(t)) = \frac{e^{b_\ell(t)}}{\sum_{\ell=1}^{L} e_\ell^b(t)},$$

$$\pi(t) = \frac{e^{c(t)}}{1 + e^{c(t)}}.$$

Then, since (as stated at beginning of Section 2) we work with discrete time points, the above dynamic systems reduce to their Euler schemes. For instance, the first equation of Eq. (4) reduces to:

$$a(t + 1) = a(t) + f_Z(a(t)).$$

Remark that, if we want to relax the condition of equally spaced points, we can introduce a parameter Δ_t such that:

$$a(t + \Delta_t) \cong a(t) + f_Z(a(t)) \cdot \Delta_t,$$

where Δ_t indicates the length of the considered time interval. Henceforth, in order to simplify the exposition, we assume that Δ_t is constant, denoted as Δ. Furthermore, for convenience, we set $\Delta = 1$ without loss of generality. A graphical representation of the model described so far, and named Zero-Inflated dLBM, can be seen in Figure 1.

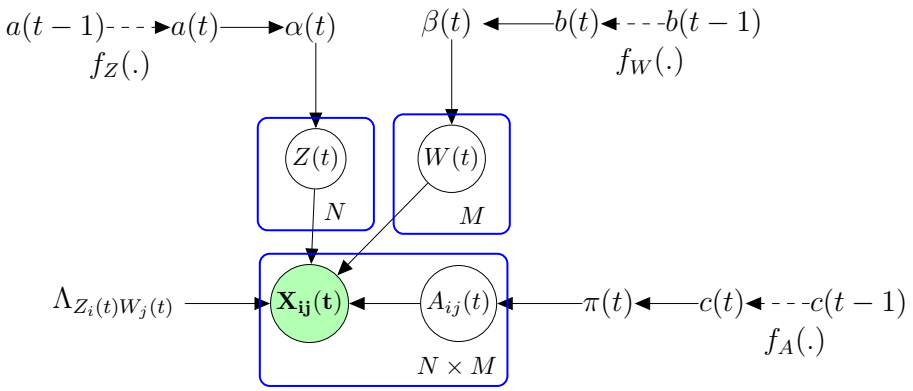

Figure 1: Graphical representation of the Zero-Inflated dLBM model.

2.3 The joint distribution

The model described so far can be adapted to any zero-inflated distribution. The first formulation as well as the most well-known concerns the Zero-Inflated Poisson, from an article by Lambert (1992). However, other distributions such as Zero-Inflated Negative Binomial (Ridout et al., 2001), Zero-Inflated Beta (Ospina and Ferrari, 2012), Zero-Inflated log-normal (Li et al., 2011) could be coupled with the present modeling.

In the following to ease the readability of the inference procedure we make use of the Zero-Inflated Poisson (ZIP) formulation to illustrate our approach. Hence, we can write $X_{ij}(t)|Z_i(t), W_j(t) \sim ZIP(\Lambda_{Z_i(t),W_j(t)}; \pi(t))$ and develop Eq. 2 as follows:

$$\begin{cases} X_{ij}(t)|Z_i(t), W_j(t) \sim \delta_0(X_{ij}(t)) & \text{with probability } \pi(t) \\ X_{ij}(t)|Z_i(t), W_j(t) \sim \mathcal{P}(\Lambda_{Z_i(t),W_j(t)}) & \text{with probability } 1-\pi(t) \end{cases}$$

where Λ is a $Q \times L$ matrix, denoting the block-dependent Poisson intensity function and $\pi(t)$ represents the sparsity at any given time period, with $t = 0, \ldots, T$.

The model described so far has a set of parameters denoted by $\theta = (\Lambda, \alpha, \beta, \pi)$ and a set of latent variables: $\{Z,\ W,\ A\}$, where $Z = \{Z(t)\}_{t=1,\ldots,T}$, $W = \{W(t)\}_{t=1,\ldots,T}$, $A = \{A(t)\}_{t=1,\ldots,T}$ and $X = \{X(t)\}_{t=1,\ldots,T}$.

As a first move, we can compute the likelihood of the complete data:

$$p(X, Z, W, A|\theta) = p(X|Z, W, A, \Lambda, \pi)p(A \mid \pi)p(Z|\alpha)p(W|\beta), \tag{5}$$

where:

$$p(X|A,Z,W,\Lambda,\pi) = \prod_{i=1}^{N}\prod_{j=1}^{M}\prod_{t=1}^{T} \mathbf{1}_{\{X_{ij}(t)=0\}}^{A_{ij}(t)} \left\{ \left(\frac{\Lambda_{Z_i(t)W_j(t)}^{X_{ij}(t)}}{X_{ij}(t)!} \exp(-\Lambda_{Z_i(t)W_j(t)}) \right)^{(1-A_{ij}(t))} \right\},$$

$$p(A|\pi) = \prod_{i=1}^{N}\prod_{j=1}^{M}\prod_{t=1}^{T} \pi(t)^{A_{ij}(t)} \Big(1-\pi(t)\Big)^{(1-A_{ij}(t))},$$

$$p(Z|\alpha) = \prod_{i=1}^{N}\prod_{q=1}^{Q}\prod_{t=1}^{T} \alpha_q(t)^{Z_{iq}(t)}, \qquad p(W|\beta) = \prod_{j=1}^{M}\prod_{\ell=1}^{L}\prod_{t=1}^{T} \beta_\ell(t)^{W_{j\ell}(t)}.$$

3 The inference algorithm

Regarding the parameter estimation, the traditional procedure for such a model would be to maximize the log-likelihood $p(X|\theta)$. However, in our case, neither the direct maximization nor the classical EM algorithm (Dempster et al., 1977; Bishop, 2006) are feasible because of the impossibility to compute the joint conditional distribution of the latent variables, $p(Z,W|X,\theta)$, due to their interdependent double missing structure. An additional difficulty in parameter estimation is also the link that α, β and π have with their respective systems of differential equations, which do not allow the formulation of a closed updating formula. This is why, we rely on the Variational-EM algorithm combined with a Stochastic Gradient Descent (SGD) optimization step. Variational inference is usually applied to complex models involving missing values or relying on latent structures (Jaakkola and Jordan, 1997; Jordan et al., 1998). The VEM algorithm has been shown to make relevant estimates of mixture models in different configurations (Govaert and Nadif, 2008).

3.1 Variational Assumption

Since we cannot compute the joint conditional distribution, $p(A,Z,W|X,\theta)$, we rely on a variational procedure which optimizes a lower bound of the likelihood. Let us thus introduce a variational distribution $q(.)$ in order to decompose the likelihood as follows:

$$\log p(X|\theta) = \mathcal{L}(q,\theta) + KL(q(.)||p(.|X,\theta)),$$

where $\mathcal{L}$ denotes a lower bound and is defined as:

$$\begin{aligned}\mathcal{L}(q,\theta) &= \sum_{Z}\sum_{W}\sum_{A} q(Z,W,A)\log\frac{p(X,A,Z,W|\theta)}{q(Z,W,A)} \\ &= E_{q(A,Z,W)}\Big[\log\frac{p(X,A,Z,W|\theta)}{q(A,Z,W}\Big] \\ &= E_{q(A,Z,W)}[\log(p(X,A,Z,W|\theta)] - E_{q(A,Z,W)}[\log(q(A,Z,W))],\end{aligned} \tag{6}$$

and KL indicates the Kullaback-Liebler divergence between the true and the approximate posterior:

$$KL(q(.)||p(.|X,\theta)) = -\sum_{A}\sum_{Z}\sum_{W} q(A,Z,W)\log\frac{p(A,Z,W|X,\theta)}{q(A,Z,W)}.$$

Now, the objective is to find a distribution $q(.)$ that maximizes the lower bound $\mathcal{L}(q,\theta)$. In order to allow the optimization of $\mathcal{L}(q,\theta)$, we further assume that $q(A,Z,W)$ factorizes as follows:

$$q(Z,W,A) = q(A)q(Z)q(W) = \prod_{i=1}^{N}\prod_{j=1}^{M}\prod_{t=1}^{T} q(A_{ij}(t))\prod_{i=1}^{N}\prod_{t=1}^{T} q(Z_i(t))\prod_{j=1}^{M}\prod_{t=1}^{T} q(W_j(t)).$$

3.2 VE-Step

The VE-step of the VEM algorithm aims at maximizing the lower bound in Eq. (6) with respect to the variational distribution $q(\cdot)$ while keeping θ fixed. Following Bishop (2006), we derive the update equations for the factors $q(A)$, $q(Z)$, and $q(W)$, such that the log of the optimized factors are given by:

$$\log q^*(A) = E_{q(W,Z)}[\log p(X,A,Z,W \mid \theta)], \tag{7}$$

$$\log q^*(Z) = E_{q(A,W)}[\log p(X,A,Z,W \mid \theta)], \tag{8}$$

$$\log q^*(W) = E_{q(A,Z)}[\log p(X,A,Z,W \mid \theta)]. \tag{9}$$

3.2.1 Optimization of the factor q(A)

Let us consider the derivation of the update equation for the factor $q(A)$. The sequential update for the factor $q(A)$ can be computed through the log of the optimized factor, where all the terms that do not depend on A are absorbed in the constant term.

Proposition 1. *Denoting by* $\delta_{ij}(t) := q(A_{ij}(t) = 1)$ *the variational success probability for* $A_{ij}(t)$*, the optimal update of* $q(A)$ *is:*

$$\delta_{ij}(t) = \frac{\exp(R_{ij}(t))}{1 + \exp(R_{ij}(t))}, \tag{10}$$

with:

$$R_{ij}(t) = \log(\pi(t)\mathbf{1}_{\{X_{ij}(t)=0\}}) + \sum_{q=1}^{Q}\sum_{\ell=1}^{L}\Big[- E_{q(W,Z)}[Z_{iq}(t)]E_{q(W,Z)}[W_{j\ell}(t)]X_{ij}(t)\log\Lambda_{q\ell} + \\ + E_{q(W,Z)}[Z_{iq}(t)]E_{q(W,Z)}[W_{j\ell}(t)]\Lambda_{q\ell}\Big] + \log X_{ij}(t)! - \log(1-\pi(t)). \tag{11}$$

The proof is provided in Appendix A. Note that, formally, when $X_{ij}(t) \neq 0$, $R_{ij}(t) = -\infty$ and $\delta_{ij}(t) = 0$, which makes sense: non-null observations in X come from a Poisson distribution with probability one (see Eq. 3).

3.2.2 Optimization of the factor q(Z)

Let us now consider the derivation of the update equation for the factor $q(Z)$. The sequential update for the factor $q(Z)$ can be computed through the log of the optimized factor, where all the terms that do not depend on Z are absorbed in the constant term.

Proposition 2. *Denoting by* $\tau_{iq}(t) := q(Z_{iq}(t) = 1)$ *the variational probability for* $Z_{iq}(t)$*, the optimal update of* $q(Z)$ *is:*

$$\tau_{iq}(t) = \frac{r_{iq}(t)}{\sum_{q_0=1}^{Q} r_{iq_0}(t)}, \tag{12}$$

with $r_{iq}(t)$ *is denoted by:*

$$r_{iq}(t) \propto \exp\left(\sum_{j=1}^{M}\sum_{\ell=1}^{L}\Big\{(1 - E_{q(A,W)}[A_{ij}(t)])\Big[E_{q(A,W)}[W_{j\ell}(t)]X_{ij}(t)\log(\Lambda_{q\ell}) - E_{q(A,W)}[W_{j\ell}(t)]\Lambda_{q\ell}\Big]\Big\} + \log(\alpha \tag{13}$$

The proof is provided in Appendix B.

3.2.3 Optimization of the factor q(W)

Let us now consider the derivation of the update equation for the factor $q(W)$. The sequential update for the factor $q(W)$ can be computed through the log of the optimized factor, where all the terms that do not depend on W are absorbed in the constant term.

Proposition 3. *Similarly for the latent variable W, denoting by $\eta_{j\ell}(t) := q(W_{j\ell}(t) = 1)$ the variational probability for $W_{j\ell}(t)$, the optimal update of $q(W)$ is:*

$$\eta_{j\ell}(t) = \frac{s_{j\ell}(t)}{\sum_{\ell_o=1}^{L} s_{j\ell_o}(t)}, \tag{14}$$

where :

$$s_{j\ell}(t) \propto \exp\left(\sum_{i=1}^{N} \sum_{q=1}^{Q} \left\{ (1 - E_{q(A,Z)}[A_{ij}(t)]) \Big[E_{q(A,Z)}[Z_{iq}(t)] X_{ij}(t) \log(\Lambda_{q\ell}) - E_{q(A,Z)}[Z_{iq}(t)] \Lambda_{q\ell} \Big] \right\} + \log(\beta_\ell(t \right. \tag{15}$$

The proof is symmetrical to the one developed for $\tau_{iq}(t)$ in Proposition 2.

3.3 Variational M-Step

In order to obtain the updating of the parameter set θ, the objective of the M-Step is the maximization of the lower bound $\mathcal{L}(q, \theta)$ with respect to $\theta = (\Lambda, \alpha, \beta, \pi)$, while holding the variational distribution $q(\cdot)$ fixed.

Proposition 4. *By developing the Eq. 6, the variational lower bound $\mathcal{L}(q, \theta)$ can be written*

as:

$$\mathcal{L}(q,\theta) = \sum_{t=1}^{T}\sum_{i=1}^{N}\sum_{j=1}^{M}\Bigg\{\delta_{ij}(t)\log(\pi(t)\mathbf{1}_{\{X_{ij}(t)=0\}}) + (1-\delta_{ij}(t))\Bigg[\log(1-\pi(t)) + \\ + \sum_{q=1}^{Q}\sum_{\ell=1}^{L}\Big\{\tau_{iq}(t)\eta_{j\ell}(t)X_{ij}(t)\log\Lambda_{q\ell} - \tau_{iq}(t)\eta_{j\ell}(t)\Lambda_{q\ell}\Big\}\Bigg] + \\ - (1-\delta_{ij}(t))\log(X_{ij}(t)!)\Bigg\} + \sum_{t=1}^{T}\sum_{i=1}^{N}\sum_{q=1}^{Q}\tau_{iq}(t)\log(\alpha_q(t)) + \\ + \sum_{t=1}^{T}\sum_{j=1}^{M}\sum_{\ell=1}^{L}\eta_{j\ell}(t)\log(\beta_\ell(t)) - \sum_{t=1}^{T}\sum_{i=1}^{N}\sum_{q=1}^{Q}\tau_{iq}(t)\log\tau_{iq}(t) + \\ - \sum_{t=1}^{T}\sum_{j=1}^{M}\sum_{\ell=1}^{L}\eta_{j\ell}(t)\log(\eta_{j\ell}(t)) - \sum_{t=1}^{T}\sum_{i=1}^{N}\sum_{j=1}^{M}\Big(\delta_{ij}(t)\log(\delta_{ij}(t)) + (1-\delta_{ij}(t))\log(1-\delta_{ij}(t))\Big). \tag{16}$$

The proof is provided in Appendix C.

3.3.1 Update of Λ

Here our goal is to derive the update of the Zero-inflated Poisson intensity parameter, Λ. The variational distribution $q(A, Z, W)$ is kept fixed, while the lower bound is maximized with respect to Λ, to obtain its update, $\hat{\Lambda}$. However, in case other zero-inflated distributions are chosen, this step must obviously be adapted to the new distribution, although the procedure of the derivation does not change.

Proposition 5. *The updating formula of Λ is obtained by maximizing $\mathcal{L}(q,\theta)$ with respect to the parameter and it can be written as follows:*

$$\hat{\Lambda}_{q\ell} = \frac{\sum_{i=1}^{N}\sum_{j=1}^{M}\sum_{t=1}^{T}\tau_{iq}(t)\eta_{j\ell}(t)\Big(X_{ij}(t) - \delta_{ij}(t)X_{ij}(t)\Big)}{\sum_{i=1}^{N}\sum_{j=1}^{M}\sum_{t=1}^{T}\tau_{iq}(t)\eta_{j\ell}(t)\Big(1-\delta_{ij}(t)\Big)}. \tag{17}$$

The proof is provided in Appendix D.

3.3.2 Update of α, β and π

The mixture proportions, $\alpha(t)$ and $\beta(t)$, and the sparsity parameter, $\pi(t)$, are driven by three systems of differential equations, in Eq. 4, respectively. As we assumed that the

functions f_A, f_W and f_Z are continuous, we propose here to parametrize them using three fully connected **neural networks** (Gent and Sheppard, 1992). Thus, optimizing the lower bound in Eq. (16) with respect to $\alpha(t)$, $\beta(t)$ and $\pi(t)$, reduces to maximize it with respect to the parameters of the neural networks, ω_A, ω_Z and ω_W, as well as to the initial values $a(0), b(0)$ and $c(0)$. In particular, we denote with $\omega(h)$ the set of weights of the neural network settled for the updating of the related parameter at iteration h. The initial set of weight is randomly sampled, $\omega(0) = \{\omega(0)\}_{k=1}^{K}$, and along the iterations they are updated, such that:

$$\omega_k(h) = \omega_k(h-1) - \gamma \nabla \mathcal{L}_{\omega_k(h)},$$

where γ is the learning rate, in the experiments they are γ_A, γ_Z, $\gamma_W = 1e-4$. The maximization is implemented in PyTorch via automatic differentiation (Paszke et al., 2017) and relies on stochastic optimisation (ADAM, Kingma and Ba, 2014). For further details on the technical details see Appendix F. Thanks to back-propagation the updated networks provide us with estimates of α, β and π. The inference procedure is summarized in Algorithm 1.

3.4 Initialization and model selection

When dealing with clustering methods based on the EM algorithm, the initialization and the selection of the appropriate numbers of clusters (for rows and columns here) are two issues which deserve an appropriate treatment. The issues related to these two points are slightly complicated here by the use of deep neural networks for modeling the dynamics of cluster and sparsity proportions. Despite this apparent difficulty due to the intrinsic complexity of these networks, they will nevertheless offer some unexpected flexibility that we may use to lower the computational cost of the whole algorithm. Indeed, and as it will be illustrated in the following numerical experiments (Section 4), the use of deep neural networks for modeling the row and column cluster proportions will allow our algorithm to work with some empty clusters.

Therefore, in the objective of avoiding the usual computationally demanding procedure of testing all pairs of row and column cluster numbers, we propose the following strategy

for both initialization and model selection.

- First, we select a single specific slice of the data $X_{t_{init}}$ and apply on it a static version of our Zip-dLBM algorithm for a list of pairs of cluster numbers, i.e. (q, ℓ) for $q = 2, \ldots, Q_{max}$ and $\ell = 2, \ldots, L_{max}$. We then use the ICL criterion (Integrated Completed Likelihood, Biernacki et al. (2000)) to select the most appropriate row and column cluster numbers for this specific slice of data. Let us remind that the ICL (Integrated Completed Likelihood) criterion aims at approximating the complete-data integrated log-likelihood and can be derived for the Zip-dLBM model as follows:

$$ICL(Q, L) = \log p(X, \hat{Z}, \hat{W}; \hat{\theta}) - \frac{Q-1}{2} \log N + \\ -\frac{L-1}{2} \log M - \frac{QL}{2} \log(NM) - \frac{1}{2} \log(NM).$$

  The pair $(\hat{Q}, \hat{L})$ that leads to the highest value for the ICL is considered as the most meaningful cluster numbers for the considered slice of data $X_{t_{init}}$. Remark that, unless a further specific notice, the slice $X_{t_{init}}$ considered for this step in our experiments will be the first slice of the data, i.e. X_{t_0}.

- Second, in order to initialize our VEM-SGD algorithm (see Algorithm 1) with useful initial values for model parameters, we initiate a cascade process as follows in order to propagate the parameter estimates obtained on the slice $X_{t_{init}}$ to the following slices. Fixing for the moment the numbers of row and column clusters to $(\hat{Q}, \hat{L})$, we run the static version of our Zip-dLBM algorithm on the next slice $X_{t_{init}+1}$ with the parameters $\hat{\theta}_{t_{init}}$ as initial values. Then, the estimated parameters $\hat{\theta}_{t_{init}+1}$ are used as initialization of the static Zip-dLBM on the slice $X_{t_{init}+2}$, and so on for the following slices. This strategy allows to provide initial values for all model parameters $\hat{\theta}(t)$, for $t = 1, ..., T$.

- Finally, as we expect that the choice of $\hat{Q}$ row and $\hat{L}$ column cluster components could not be the best for all slices of the data set, the VEM-SGD algorithm (see Algorithm 1) will be then run with more components than considered in the initialization. Indeed, we run the VEM-SGD algorithm with $Q_{max} \geq \hat{Q}$ and $L_{max} \geq \hat{L}$

cluster components. Then, part of the model parameters are initialized with $\hat{\theta}(t)$ obtained via the initialization procedure described above (see Algorithm 2) and the remaining parameters, corresponding to the additional row and column clusters are set to zero. Thus, we aim at exploiting the potential "blessing" of the use of deep neural networks allowing our VEM-SGD algorithm to start with some empty clusters. These empty clusters will have the possibility to be activated later in the inference process, if needed. Therefore, we avoid the usual computationally demanding procedure of running the whole algorithm with all pairs of row and column cluster numbers for the whole data set. This strategy allows our approach to scale to massive data sets in a reasonable computation time and with satisfying results, as it will be illustrated in the next section. Similar propositions within the Bayesian framework have been proposed by Malsiner-Walli et al. (2016) in their work on model-based clustering based on sparse finite Gaussian mixtures and by Forbes et al. (2019) where two strategies are proposed for selecting the number of components in non-Gaussian mixture models.

4 Numerical experiments

The main purpose of this section is to highlight the most important features of our zero-inflated dLBM algorithm over simulated data sets in the Poisson scenario. We aim at demonstrating the validity of the inference algorithm and model selection criterion presented in the previous sections. The first experiment consists in applying Zip-dLBM to a specific data set with evolving block pattern and sparsity to show that it recovers the data structure. The second experiment shows that Zip-dLBM is able to uncover clusters being initially empty, filling up over time, then emptying again. The third experiment shows the robustness of Zip-dLBM when the initial number of clusters is not the actual one, thus testing the performance of the model in case of poor initialization. The fourth experiment demonstrates the model selection procedure on 50 simulated date sets. All the experiments on simulated data were realized on data sets with $N = 600$ rows, $M = 400$ columns and $T = 50$ time instants. In Section G, other experiments on simulated data are proposed,

namely a benchmark study and an experiment to asses the robustness model assumption.

4.1 Introductory example

As a first example, we simulate a data set with dimension $600 \times 400 \times 50$ and with $Q = 3$ groups of rows, $L = 2$ groups of columns. The level of sparsity ranges from 80% to 90% in the time period. The values of the other simulated parameters in this experiment are shown in Table 1.

Cluster	α	β
1	0.2 to 0.8	0.1 to 0.99
2	0.18 to 0.14	0.99 to 0.1
3	0.6 to 0.06	-

$$\Lambda = \begin{bmatrix} 6 & 4 \\ 1 & 2 \\ 7 & 3 \end{bmatrix}$$

Table 1: Mixing proportion and Λ values.

We apply Zip-dLBM to the simulated data set with the actual values of Q and L to show the ability of the model to fully recover the model parameters. The running time for this experiment is 23.5 minutes on CPU on a MacBook Pro, 2020, with a processor of 2,3 GHz Quad-Core Intel Core i7 and 16 GB of RAM (see Section F of the Appendix for details).

Figure 2 shows the evolution of the the lower bound, expressed in Eq. 16, that Zip-dLBM aims to maximize. We can notice the convergence is reached in less than 10 iterations. It is worth noticing that each iteration of the algorithm involves the optimization through gradient descent of the loss for 2000 epochs, for each parameter. In this example Figure 4 shows the evolution of the estimated mixture parameters $\hat{\alpha}$, $\hat{\beta}$ and $\hat{\pi}$ along the time period, represented on the x-axes. These parameters are estimated through the stochastic gradient descent technique, linked with the neural networks. By looking at these figures, we see the true parameters on the left column, the output of the initialization procedure in the middle and the results the Zip-dLBM estimates on the right. The comparison between the simulated and estimated parameter evolution shows that the model fully recovers the actual values over time, modulo the switched labels for the mixture proportions.

Figure 3, displays the reorganized incidence matrices at time instants $t = 10$ and $t = 30$, respectively.: the rows and columns of the incidence matrix are permuted according to the estimates of the latent variables $\hat{Z}$ and $\hat{W}$, in such a way that nearby rows (columns) belong to the same cluster of rows (columns). The blocks are also delimited by black dashed lines. The density of points within each block is determined by the intensity function of the Poisson distribution, represented by the parameter matrix Λ. The estimated values of Λ are as follows:

$$\Lambda = \begin{bmatrix} 3.001 & 7.001 \\ 2.000 & 1.004 \\ 3.990 & 5.998 \end{bmatrix}.$$

As expected, our algorithm succeeds to recover the simulated pattern. The similarity between the estimated and simulated values validates the accuracy of our modeling approach in capturing the underlying patterns and characteristics of the data, modulo the switched orders. Furthermore, to evaluate the quality of the clustering, we use a measure called CARI, recently introduced by Robert et al. (2021a). This new criterion is based on the Adjusted Rand Index (Rand, 1971) and it was developed especially for being applied to co-clustering methods. The closer the index is to 1, the more both the row and column partitions are close to the actual ones, whereas the closer the value is to 0, the greater the difference between the true and estimated labels. In this experiment we obtained a CARI index of 1. From these results we can clearly see that our algorithm perfectly identifies the composition of the original clusters and it recovers the evolution of the mixing proportion over time.

4.2 Robustness of the initialization procedure

In this section we perform two experiments to test the robustness of the model to initialization. In the first experiment, we initialize parameters with wrong number of clusters, while in the second experiment the data are simulated with particularly complex dynamics. In fact, we test the model's ability to identify a cluster that is empty at the beginning of the

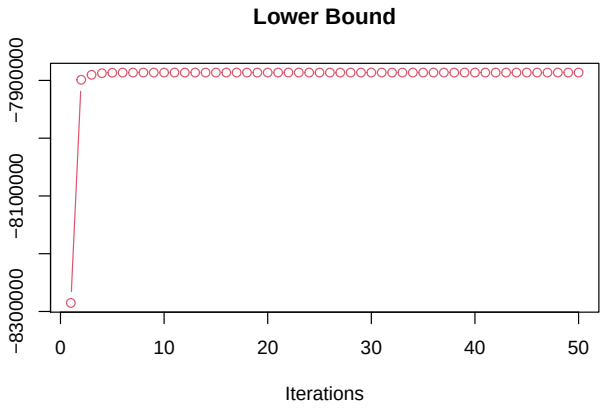

Figure 2: Lower bound maximization throughout the iterations of the Zip-dLBM algorithm.

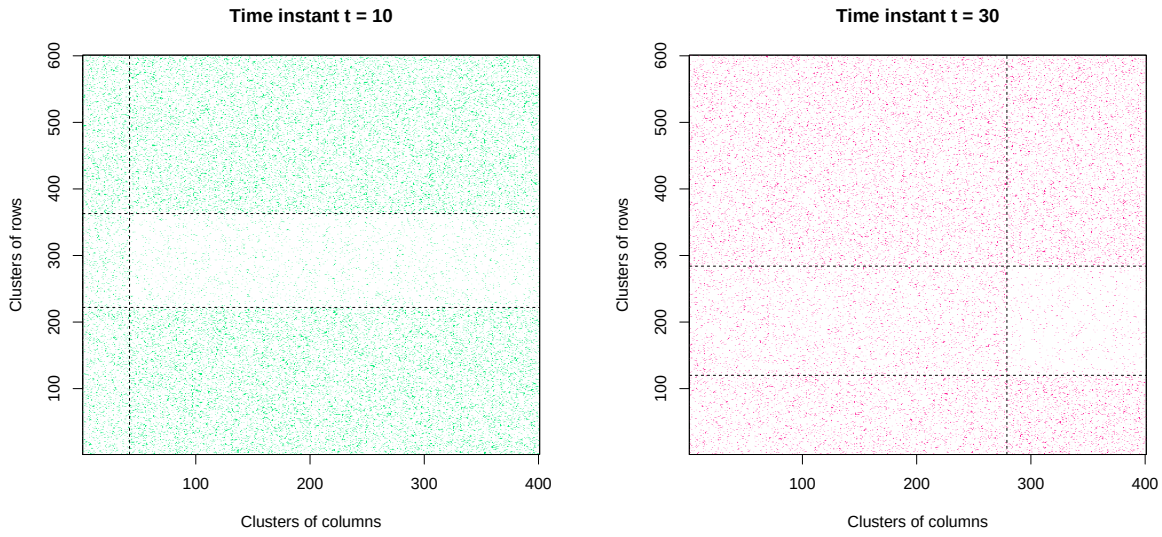

Figure 3: Reorganized incidence matrices at time instants $t = 10$ and $t = 30$ according to the estimates of the cluster memberships. Nearby rows (columns) belong to the same cluster of rows (columns). The blocks are also delimited by black dashed lines.

period, which fills up and then empties again. As for the first experiment to test the robustness of our initialization strategy, Zip-dLBM was intentionally initialized with a higher than the optimal number of clusters. In fact, although the data were simulated with $Q = 3$ and $L = 2$, both the initialization process and Zip-dLBM were run with $Q = 5$ and $L = 4$. Figure 5 shows on the left column the evolution of the simulated mixture proportions and

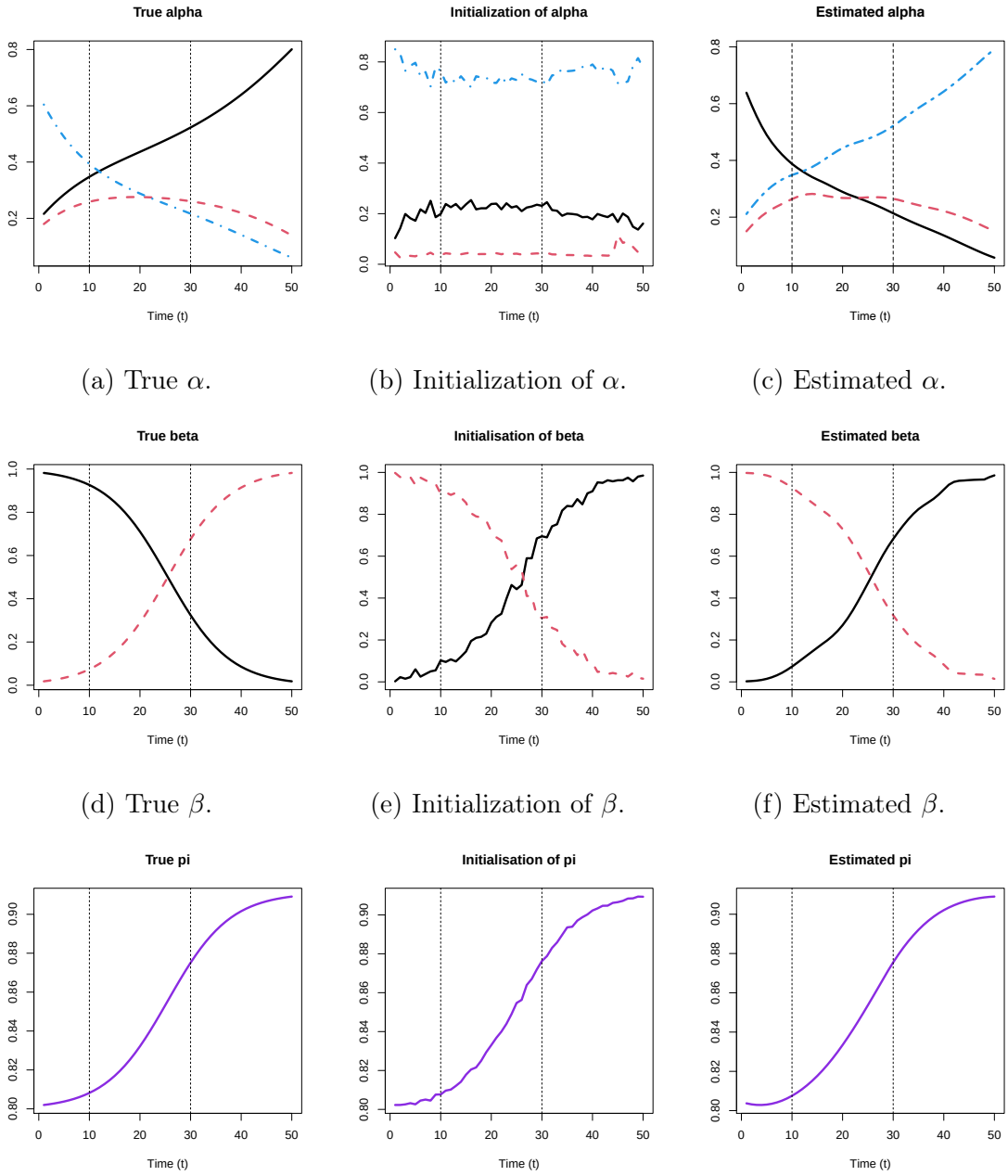

(a) True α. (b) Initialization of α. (c) Estimated α.

(d) True β. (e) Initialization of β. (f) Estimated β.

(g) True π. (h) Initialization of π. (i) Estimated π.

Figure 4: Evolution of the true (left), initialized (center) and estimated (right) proportions of the parameters α, β and π, respectively. Each curve represents the evolution of a column (row) cluster proportion.

the sparsity parameter, in the middle column their initialization, and on the right column the results of the estimates provided by Zip-dLBM. We can see that the initialization of α in Figure 5b is rather poor. Nevertheless, Zip-dLBM finds the right trend of the mixture proportions over time, effectively emptying the two superfluous clusters.

In this experiment a CARI index value was calculated for each time instant; the obtained CARI index is 0.98.

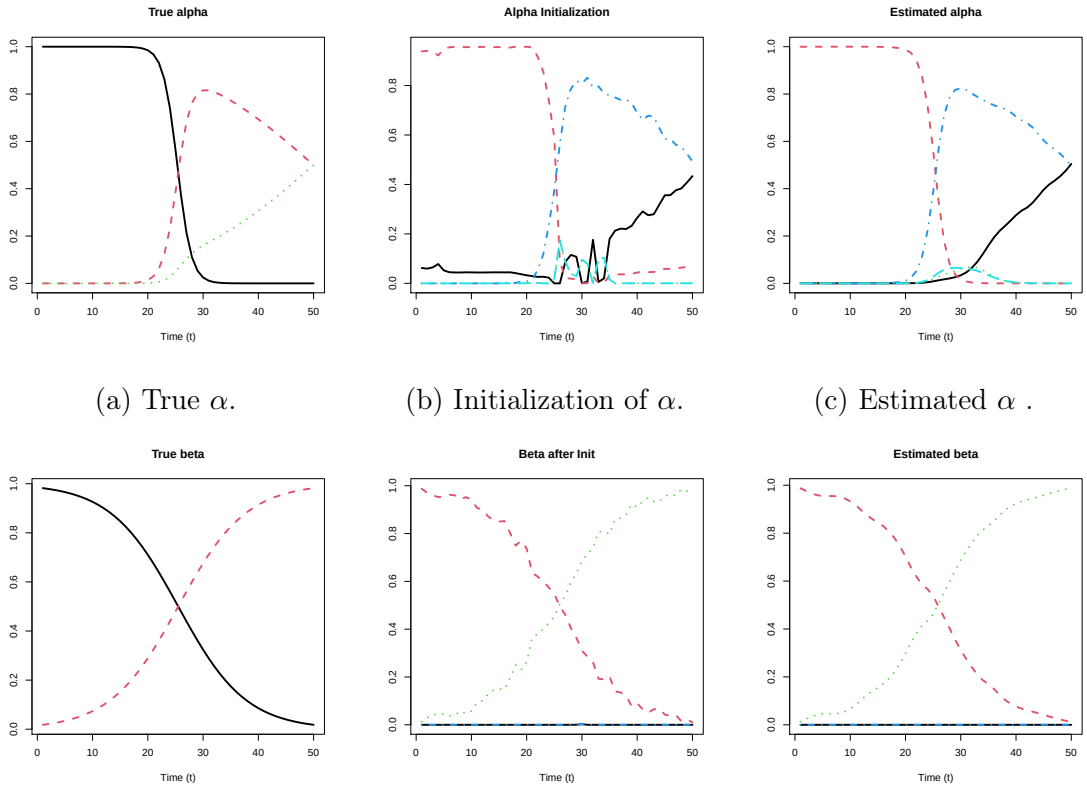

(a) True α. (b) Initialization of α. (c) Estimated α .

(d) True β. (e) Initialization of β. (f) Estimated β.

Figure 5: Evolution of the true (left), initialized (center) and estimated (right) group proportions of the parameters α and β, respectively. Each curve represents the evolution of a column (row) cluster proportion.

Now, as for the second experiment of testing the robustness of the model to initialization, we simulate the data in such a way that in the clusters in line there is one that is empty at the beginning of the period under consideration, then fills up towards the middle of the

period, and then empties again at the end, Figure 6a shows this dynamic. Through this experiment we want to show how Zip-dLBM is able to find the right evolution of mixture proportions despite the complex dynamics. Figure 6 depicts the simulated parameters on the left, the initial estimates in the middle, and the final estimates on the right. Looking at the middle part, in Figure 6b, we can see that the initialization process is not particularly helpful to the model because of the switched labels and a poor parameters estimation. Despite the initialization, we see in Figure 6c that Zip-dLBM is perfectly able to recognize the initially empty cluster which then gradually fills up and empties again. In this experiment, the CARI index, obtained by averaging the indexes over time, is 0.95.

4.3 Model selection experiment

Previous experiments have allowed us to attest that the initialization strategy is globally robust and that the application of Zip-dLBM allows us to correct for poor initializations with respect to the number of clusters in rows or columns. Therefore, in this experiment we test the global capability in choosing the optimal number of clusters in rows and columns over a larger number of simulated datasets through the combination of the initialization procedure and the application of the Zip-dLBM algorithm. Let us recall that, as mentioned in Section 3, the ICL criterion identifies the optimal number of clusters only at one time instant in order to initialize the parameters optimally. Subsequently, Zip-dLBM is run with a higher number of clusters than those identified by ICL. Hence, to validate the performances on the component activation, 50 independent data sets are generated with the setup explained in Section 4.1, with $Q = 3$ row clusters and $L = 2$ column clusters, a level of sparsity varying between 80% and 90% and the other model parameters equal to:

Cluster	α	β
1	0.2 to 0.8	0.1 to 0.99
2	0.18 to 0.14	0.99 to 0.1
3	0.6 to 0.06	-

$$\Lambda = \begin{bmatrix} 6 & 4 \\ 1 & 2 \\ 7 & 3 \end{bmatrix}$$

Table 2: Mixing proportion and Λ values.

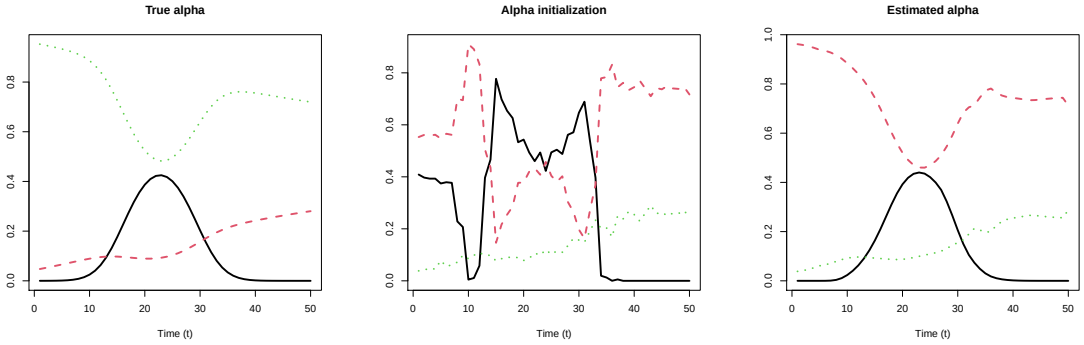

(a) True α. (b) Initialization of α. (c) Estimated α.

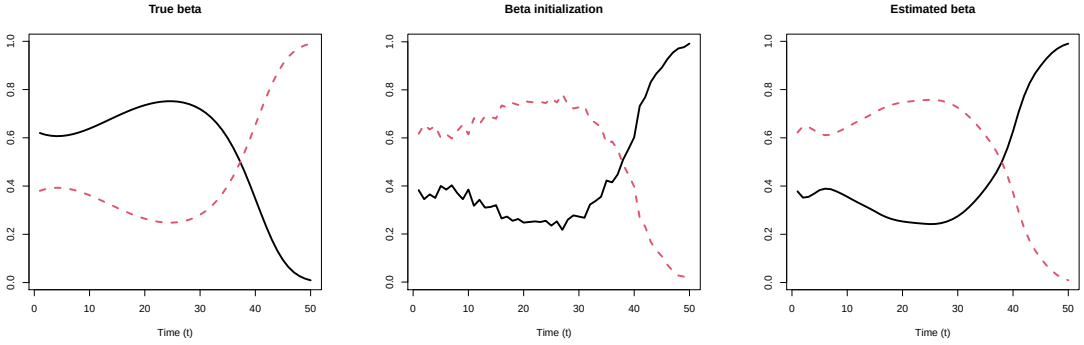

(d) True β. (e) Initialization of β. (f) Estimated β.

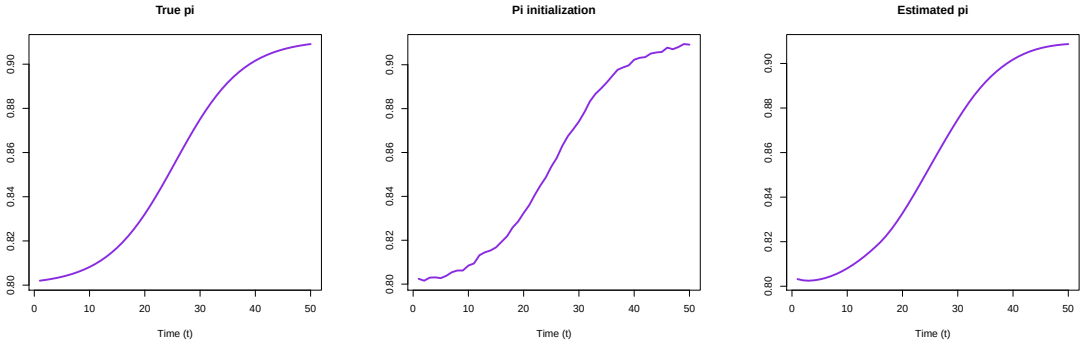

(g) True π. (h) Initialization of π. (i) Estimated π.

Figure 6: Evolution of the true (left), initialized (center) and estimated (right) proportions of the parameters α, β and π, respectively. In figures (a) to (f), each curve represents the evolution of a column (row) cluster proportion, while figures g to i represent the true (left), initialized (center) and estimated (right) parameter π.

Then, Zip-dLBM is applied on those simulated data sets using values of Q and L equal to 10. Table 3 shows the percentage of selections. The highlighted cell corresponds to the actual value of Q and L. Zip-dLBM succeeds 86% of the time to identify the correct model. Specifically, to evaluate the results of this experiment, we averaged the membership probability of the two estimated mixing parameters, α and β; exceeding clusters having an average membership probability of less than 1e-3 were considered to be off. Among the results of the 50 simulated data sets, we report in Figure 7, as an illustrative example, one of the component activation results. We see that not only the unnecessary clusters remained empty, but also the estimates of the α and β are good, as Zip-dLBM manages to identify the evolution of the two mixing parameters over time, despite the number of clusters given as input is not the optimal one.

Q/L	1	2	3	4	5	6	7	8	9	10
1	0	0	0	0	0	0	0	0	0	0
2	0	0	0	0	0	0	0	0	0	0
3	0	86	0	0	0	0	0	0	0	0
4	0	2	0	0	0	0	0	0	0	0
5	0	2	0	0	0	0	0	0	0	0
6	0	0	0	0	0	0	0	0	0	0
7	0	0	0	0	0	0	0	0	0	0
8	0	4	0	0	0	0	0	0	0	0
9	0	2	0	0	0	0	0	0	0	0
10	0	4	0	0	0	0	0	0	0	0

Table 3: Model selection. Percentage of activated components on 50 simulated data sets. The highlighted cell corresponds to the actual value of Q and L.

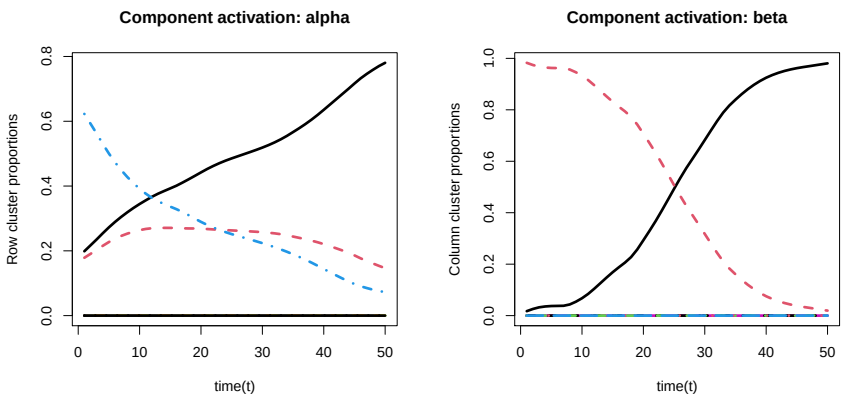

Figure 7: View of a model selection result: the useful clusters are activated while the useless ones lie empty on the basis of the figure.

5 London bike sharing

This section focuses on the application of Zip-dLBM to a large-scale bike-sharing data set in London, with the aim of illustrating the potential of our tool on a real data set.

5.1 Protocol and data

The data are collected and publicly distributed by Transport for London[3] We focus on one-month, specifically June 2022, as it represents in our view a neutral choice for the use of shared bikes, both regarding the end of Covid pandemic and the weather conditions. The objective of this application is to analyze how inbound (Arrival) and outbound (Departure) bike rental stations take on different roles, and, consequently, different cluster memberships, depending on the hour of the day. To analyze the data, we summed up the hourly interactions on the working days of the month, in order to order to obtain a "cumulative" day that we consider from 6 am to 10 pm. So, the time unity measure is one hour and the overall data set is made of by 776,270 observations, for which we consider the departure station name, the arrival station name and the start time date. Moreover, we

[3] `https://cycling.data.tfl.gov.uk`, also available on GitHub at: `https://github.com/giuliamar95/Zip-dLBM` and in the Supplementary Materials.

only consider stations (arrival and departure) that were rented more than 50 times over the month of June 2022. The resulting data set contains 791 departure stations, 791 arrival stations and 16 hours corresponding to 475,586 non-zero entries in the incidence matrix. Figure 8 represents the number of bikes in use in the London sharing system at every hour over the whole month of June. It can be clearly noticed that there are two peaks at the rush hours when people go to or from work (7-8 am and 5-6 pm).

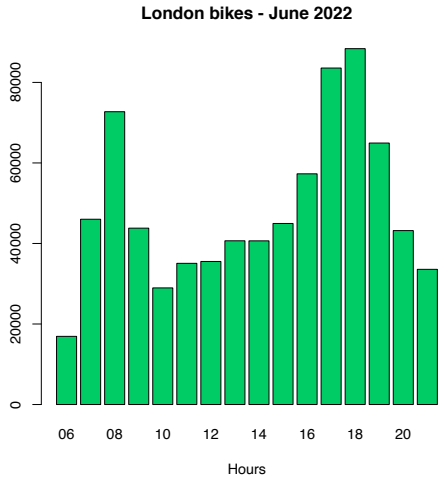

Figure 8: Barplot of the number of bikes taken from the London sharing system, from 6 am to 10 pm, in a cumulative day, corresponding to June 2022.

5.2 Summary of the results

We fit Zip-dLBM to the data with a running time of 22.3 minutes on CPU on a MacBook Pro, 2020, with a processor of 2,3 GHz Quad-Core Intel Core i7 and 16 GB of RAM (see Section F of the Appendix for details). For the initialization, as explained in Section 3.4, we computed the ICL criterion on one data slice, corresponding on the hour 9 am - 10 am, where the optimal number of clusters identified by the model selection criterion are $\hat{Q} = 6$ and $\hat{L} = 6$. Then, we initiated the model parameters through the cascade process described in Algorithm 2 and we ran Zip-dLBM with $Q = 10$ and $L = 10$ to allow the model to fill or empty clusters as needed.

Figure 9 represents the estimated Poisson intensities Λ for Zip-dLBM. This figure only focuses on the 6 groups of departure stations, denoted by the letter D, and the 6 groups of arrival stations, denoted by the letter A, that have been activated in the inference. Each color refers to a departure (rows) or arrival (columns) cluster and the higher is the value in each block, the strongest is the relationship (i.e the expected number of bikes exchanged in the time unit) between the related pair of clusters. Looking at this figure, it can be

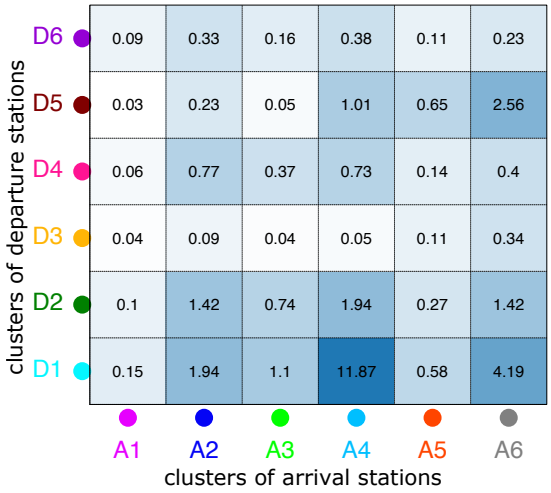

Figure 9: Estimated Poisson intensity function, each color represents a different departure (arrival) cluster.

seen that some clusters are strongly related whereas others are not at all. For example, cluster D1 (light blue) of the departure stations is highly related with clusters A4 and A6 of arrival stations. Also, cluster D5 of departure stations shows the same behavior but with lower intensity levels. Hence, one may think that the arrival clusters A4 and A6 are located in the city center or in highly busy areas. This intuition is supported by Figure 1 in Appendix A, where an animation showing the evolution of cluster composition and position over the day is depicted. In fact, looking at these figures one can see that cluster D1 of the departure stations is mostly concentrated at central locations and, more specifically, at the stations emitting the highest number of bikes, such as Hyde Park, King's Cross, and Queen Elizabeth Olympic Park. We also noted that during the month of June 2022

in Hyde Park and Queen Elizabeth Olympic Park several major events were held, such as the Rolling Stones concert (Hyde Park) and the Red Hot Chili Peppers concert (Queen Elizabeth Olympic Park). This suggests that this cluster includes stations that are subject to a higher-than-normal load. Also, from Figure 1 in Appendix A, we can see a particular behavior of cluster D2 (green) of outgoing bikes. This cluster is characterized by bikes leaving the suburbs during the morning peak hours (7 am-9 am) and then concentrating more in the city center during the day and especially in the evening rush hours (4 pm-6 pm). In addition, this cluster has a strong relationship with clusters A2, A4 and A6 of arrival stations. Among them, clusters A4 and A6 represent mostly central stations, while cluster A2 is concentrated in the city center in the morning rush hours and in the suburbs in the evening rush hours. We might infer that this dynamic is typical of workers who decide to bike to their workplaces. On the contrary, clusters D3 and D6 of departure stations have a very low intensity of interactions with the arrival clusters, however they are really spread all over the city. In particular, cluster D3 has the highest level of interactions with cluster A6 of arrival stations, while cluster D6 has the highest intensity level with cluster A2 and cluster A4 of arrival stations. The main difference between clusters D3 and D6 concerns their location. In fact, all over the day, there are really few points belonging to cluster D3 and they are mainly concentrated in the Greenwich peninsula and, only at the end of the day, in the city center. Cluster D6, on the contrary, concentrates in the city center and in some specific areas, such as Greenwich peninsula, Wandworth and Sheperd's Bush early in the morning, then it spreads all over the city. Therefore, from the large initial data matrix, Zip-dLBM was able to identify consistent and relevant clusters of the London sharing bike. stations

5.3 Interpretation of the estimated parameters

To better understand the results, we now focus on the estimates of the other model parameters. Figure 10 shows the estimated evolution of the sparsity parameter over time. We see that, at the beginning of the day, 6 am, the sparsity is at 95%, then as we approach the morning peak, the number of borrowed sharing bikes increases and consequently the

sparsity decreases, reaching 86% at 8 am. Between 9 am and 2 pm, it again increases slightly (90%) and then decreases as we approach the peak at the end of the day, when workers leave work. In fact, at 6 pm the sparsity level reaches its daily minimum at a level of 80%.

Figures 11a and 11b show the estimation of the mixing parameters α and β. From Figure 11a, we see how cluster D2 has a precise evolution, corresponding to the daily work rhythm. Cluster D4 and Cluster D6 on the contrary, have exactly the opposite behavior, filling up in the non-rush hours of the day, starting at 10 am, then emptying out in the rush hour of the afternoon and filling up again in the evening. We might infer that the outbound bikes in these clusters are mostly rented by tourists. Cluster D1, on the other hand, as mentioned earlier, is very peculiar because it contains a few stations that emit a lot of bikes, probably when there are special events that mobilize a large number of people. (e.g concerts, football matches, etc.)

Looking at Figure 11b instead, we see estimates of the mixing proportions of the arrival bike clusters. Cluster A2 again has the typical workday evolution, thus including those bike stations taken to get to the workplace and back home at the end of the day. Another particular group is cluster A3. Its proportions increase from 10 am reaching a peak between 2 pm and 3 pm, and while all other clusters tend to empty out in the evening, this one increases. Cluster A5 fills in mid-morning and then remains stable during the rest of the day. Clusters A4 and A6, on the other hand, are very small in terms of proportions. As we saw earlier, they in fact include few but very central stations with a very high density of interactions.

5.4 Insights into the evolution of two departure and arrival clusters

For pedagogical purposes, in this section we choose two clusters, specifically the departure bike cluster D2 and the arrival bike cluster A2, by analyzing the results in detail. Figure 12 depicts cluster D2 of the departing stations and its evolution in 3 time instants: 7 am, 1 pm and 6 pm. As mentioned, given its specific dynamics, this cluster is likely to be populated

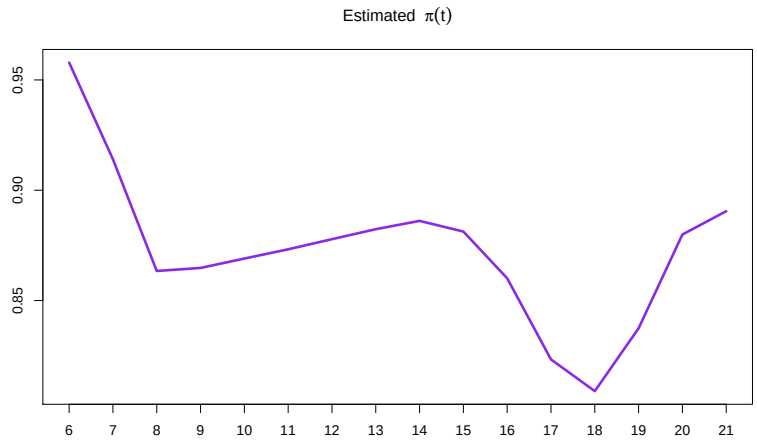

Figure 10: Evolution of $\hat{\pi}$ estimation.

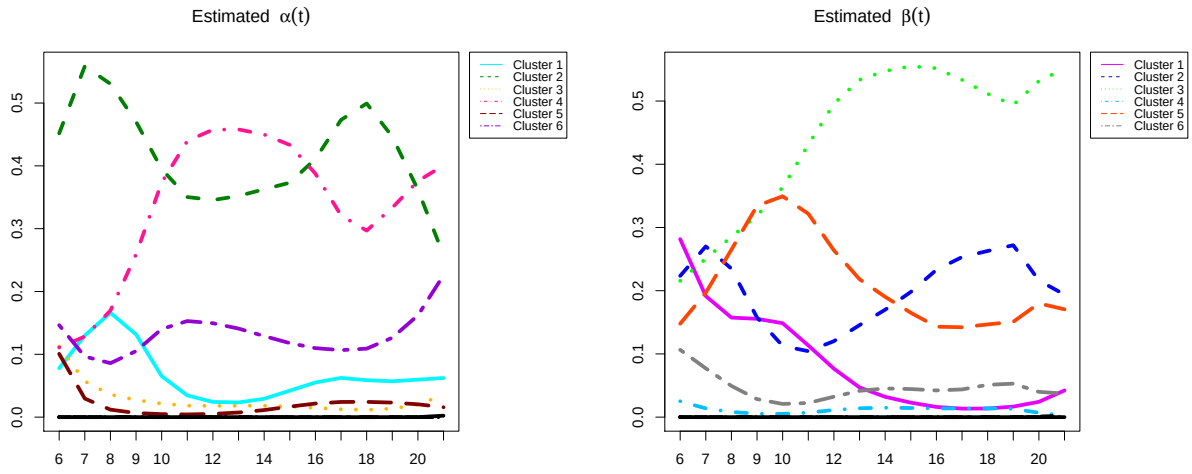

(a) Evolution of the estimates $\hat{\alpha}$.

(b) Evolution of the estimates $\hat{\beta}$.

Figure 11: Evolution of the estimates $\hat{\alpha}$ and $\hat{\beta}$, indexing the cluster proportions of departure and arrival stations, respectively. Each color represents a different cluster.

by bicycle stations used mostly by workers. In fact, in Figure 12a we see that at 7 am there are many points, mostly distributed outside the city center. Thereafter, around 1 pm (Figure 12b) the volume of points decreases. Then, toward the afternoon rush hour, in Figure 12c, the density of points increases again. Indeed, in Figure 12c we see that most of the points are now located in the center. This behavior is typically due to the workers

from the suburbs going to work in the city center while at the end of the day taking the shared bikes back to leave the city center.

Similarly, Figure 13 shows the cluster A2 of the arrival stations and its evolution in 3 time instants: 7 am, 1 pm and 6 pm. Here we note how at 7 am cluster A2 contains arrival stations all located in the city center. In contrast, in Figure 13b, the number of bikes belonging to this cluster decreases and the locations are more scattered. Whereas, in Figure 13c, we note how at the end of the workday, most of the arrival stations in this cluster are no longer located in the center but in the suburbs. Thus, from the comparison of Figure 12 and Figure 13 we notice a complementary trend, dictated by the fact that the arrival and departure stations in the two selected clusters are both characteristic of the daily work schedules.

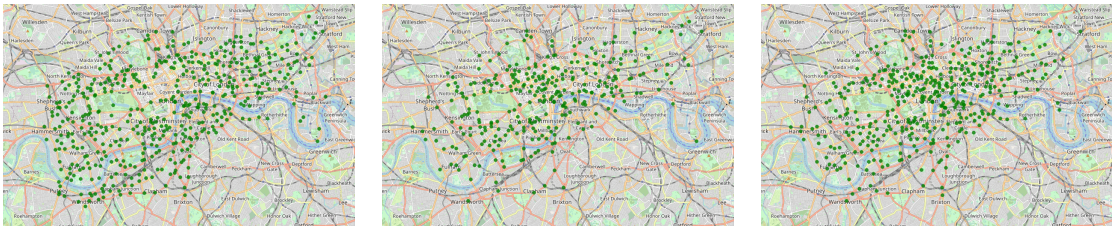

(a) Cluster D2 - 7 am. (b) Cluster D2 - 1 pm. (c) Cluster D2 - 6 pm.

Figure 12: Snapshots of the evolution of the departure cluster D2 at three different times in the day: 7 am, 1 pm, 6 pm.

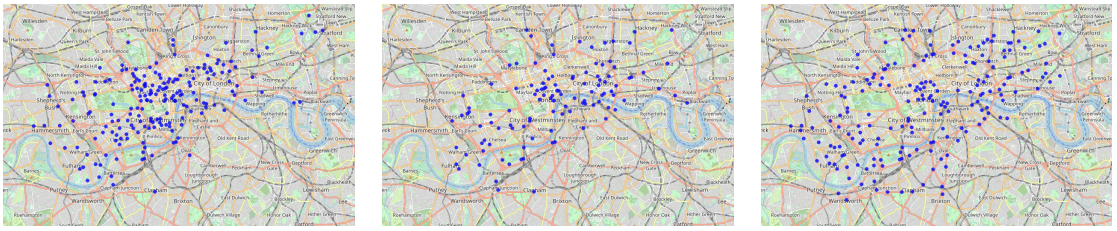

(a) Cluster A2 - 7 am. (b) Cluster A2 - 1 pm. (c) Cluster A2 - 6 pm.

Figure 13: Snapshots of the evolution of the arrival cluster A2 at three different times in the day: 7 am, 1 pm, 6 pm.

6 Conclusion

This work is born out of the need to analyze and summarize observations and features of a dynamic matrix in a simultaneous way. We have proposed a dynamic co-clustering technique, with the purpose of simultaneously performing clustering of rows and columns along the time dimensions. Since observations and features are allowed to change their cluster memberships in time, it is of great interest to look for structural changes in the way clusters interact with each other along the considered time period. We have introduced a generative zero-inflated dynamic latent block model, that can be further adapted to several zero-inflated probability distributions. For ease of reading the mathematical and experimental part, in this paper we used the Zero-Inflated Poisson distribution, thus introducing the Zero-Inflated Poisson Dynamic Latent Block model (Zip-dLBM). The time modeling relies on three systems of ordinary differential equations. Inference is done using a Variational EM algorithm together with stochastic optimization for the parameters of the dynamic systems. The performance of our approach, called Zip-dLBM in the Poisson case, is evaluated through applications to several simulated data scenarios and compared with competing methods. Then, Zip-dLBM was fitted to a large-scale real data set, the London sharing bikes. In this context, Zip-dLBM provided meaningful and interpretable results. As a further work, it would be of interest to develop a online inference algorithm for Zip-dLBM, to be used as a real-time co-clustering tool. It would also be interesting to do some real-time change point detection, with possible applications to data from several domains (transportation or medical, for instance). A further idea would be to introduce dynamic systems also for the variational parameters, in the inference model. However, this choice might be very computationally expensive and require further investigation.

Acknowledgements

This work has been supported by the French government, through the 3IA Côte d'Azur, Investment in the Future, project managed by the National Research Agency (ANR) with the reference number ANR-19-P3IA-0002.

Conflict of Interest

The authors report there are no competing interests to declare.

Appendix

A Proof: Optimization of the factor q(A)

Starting from Eq. 7, we use the decomposition in Eq. 5, and then we substitute the conditional distributions on the right-hand side. We denote by *const* those terms in the lower bound not depending on $A_{ij}(t)$.

$$
\begin{aligned}
\log(q^*(A)) &= E_{q(W,Z)}[\log(p(X,Z,W,A|\theta)] + const; \\
&= E_{q(W,Z)}[\log(p(X|Z,W,A,\Lambda,\pi)] + E_{q(W,Z)}[\log(A|\pi)] + const \\
&= \sum_{i=1}^{N}\sum_{j=1}^{M}\sum_{t=1}^{T}\Bigg\{ A_{ij}(t)[\log \mathbf{1}_{\{X_{ij}(t)=0\}}] + (1-A_{ij}(t))\Bigg[\sum_{q=1}^{Q}\sum_{\ell=1}^{L}\Big[E_{q(W,Z)}[Z_{iq}(t)]E_{q(W,Z)}[W_{j\ell}(t)]X_{ij}(t)\log\Lambda_{q\ell} \\
&- E_{q(W,Z)}[Z_{iq}(t)]E_{q(W,Z)}[W_{j\ell}(t)]\Lambda_{q\ell}\Big] - \log X_{ij}(t)!\Bigg] + A_{ij}(t)\log\pi(t) + (1-A_{ij}(t))\log(1-\pi(t))\Bigg\} + const \\
&= \sum_{i=1}^{N}\sum_{j=1}^{M}\sum_{t=1}^{T}\Bigg\{ A_{ij}(t)\log\pi(t)\mathbf{1}_{\{X_{ij}(t)=0\}} + (1-A_{ij}(t))\Bigg[\sum_{q=1}^{Q}\sum_{\ell=1}^{L}\Big[E_{q(W,Z)}[Z_{iq}(t)]E_{q(W,Z)}[W_{j\ell}(t)]X_{ij}(t)\log\Lambda_{q\ell} \\
&- E_{q(W,Z)}[Z_{iq}(t)]E_{q(W,Z)}[W_{j\ell}(t)]\Lambda_{q\ell}\Big] - \log X_{ij}(t)! + \log(1-\pi(t))\Bigg]\Bigg\} + const \\
&= \sum_{i=1}^{N}\sum_{j=1}^{M}\sum_{t=1}^{T}\Bigg\{ A_{ij}(t)\log\pi(t)\mathbf{1}_{\{X_{ij}(t)=0\}} + A_{ij}(t)\Bigg[\sum_{q=1}^{Q}\sum_{\ell=1}^{L}\Big[-E_{q(W,Z)}[Z_{iq}(t)]E_{q(W,Z)}[W_{j\ell}(t)]X_{ij}(t)\log\Lambda_{q\ell} \\
&+ E_{q(W,Z)}[Z_{iq}(t)]E_{q(W,Z)}[W_{j\ell}(t)]\Lambda_{q\ell}\Big] + \log X_{ij}(t)! - \log(1-\pi(t))\Bigg]\Bigg\} + const \\
&= \sum_{i=1}^{N}\sum_{j=1}^{M}\sum_{t=1}^{T}\Bigg\{ A_{ij}(t)\Bigg[\log\pi(t)\mathbf{1}_{\{X_{ij}(t)=0\}} + \sum_{q=1}^{Q}\sum_{\ell=1}^{L}\Big[-E_{q(W,Z)}[Z_{iq}(t)]E_{q(W,Z)}[W_{j\ell}(t)]X_{ij}(t)\log\Lambda_{q\ell} \\
&+ E_{q(W,Z)}[Z_{iq}(t)]E_{q(W,Z)}[W_{j\ell}(t)]\Lambda_{q\ell}\Big] + \log X_{ij}(t)! - \log(1-\pi(t))\Bigg]\Bigg\} + const.
\end{aligned}
$$

We can then recognize the functional form of the Bernoulli distribution by indicating:

$$
\begin{aligned}
\log q^*(A) &\propto \sum_{i=1}^{N}\sum_{j=1}^{M}\sum_{t=1}^{T} A_{ij}(t)\log\delta_{ij}(t) + (1-A_{ij}(t))\log(1-\delta_{ij}(t)), \\
&\propto \sum_{i=1}^{N}\sum_{j=1}^{M}\sum_{t=1}^{T} A_{ij}(t)\frac{\log\delta_{ij}(t)}{1-\log\delta_{ij}(t)}
\end{aligned}
$$

where $\delta_{ij}(t)$ is defined as:

$$
\delta_{ij}(t) = \frac{\exp(R_{ij}(t))}{1+\exp(R_{ij}(t))},
$$

with $R_{ij}(t)$ defined as:

$$R_{ij}(t) = \log(\pi(t)\mathbf{1}_{\{X_{ij}(t)=0\}}) + \sum_{q=1}^{Q}\sum_{\ell=1}^{L}\Big[- E_{q(W,Z)}[Z_{iq}(t)]E_{q(W,Z)}[W_{j\ell}(t)]X_{ij}(t)\log\Lambda_{q\ell} +$$
$$+ E_{q(W,Z)}[Z_{iq}(t)]E_{q(W,Z)}[W_{j\ell}(t)]\Lambda_{q\ell}\Big] + \log X_{ij}(t)! - \log(1-\pi(t)).$$

B Proof: Optimization of the factor q(Z)

Starting from Eq. 8, we use the decomposition in Eq. 5, and then we substitute the conditional distributions on the right-hand side. We denote by *const* those terms in the lower bound not depending on $Z_{iq}(t)$.

$$\begin{aligned}
\log q^*(Z|\theta) &= E_{q(A,W)}[\log p(X,A,Z,W \mid \theta)] \\
&= E_{q(A,W)}[\log(p(X \mid A,Z,W,\Lambda,\pi) + \log p(Z \mid \alpha)] \\
&= E_{q(A,W)}\Bigg[\sum_{i=1}^{N}\sum_{j=1}^{M}\sum_{t=1}^{T}\Bigg\{(1-A_{ij}(t))\sum_{q=1}^{Q}\sum_{\ell=1}^{L}\Big\{Z_{iq}(t)W_{j\ell}(t)X_{ij}(t)\log(\Lambda_{q\ell}) - Z_{iq}(t)W_{j\ell}(t)\Lambda_{q\ell}\Big\} \\
&- (1-A_{ij}(t))\log(X_{ij}(t)!)\Bigg\}\Bigg] + \sum_{i=1}^{N}\sum_{q=1}^{Q} Z_{iq}(t)\log(\alpha_q(t)) + \text{const}, \\
&= \sum_{i=1}^{N}\sum_{j=1}^{M}(1-E_{q(A,W)}[A_{ij}(t)])\Bigg[\sum_{q=1}^{Q}\sum_{\ell=1}^{L}\Big\{Z_{iq}(t)E_{q(A,W)}[W_{j\ell}(t)]X_{ij}(t)\log(\Lambda_{q\ell}) + \\
&- Z_{iq}(t)E_{q(A,W)}[W_{j\ell}(t)]\Lambda_{q\ell}\Big\}\Bigg] + \sum_{i=1}^{N}\sum_{q=1}^{Q} Z_{iq}(t)\log(\alpha_q(t)) + \text{const}, \\
&= \sum_{i=1}^{N}\sum_{q=1}^{Q} Z_{iq}(t)\Bigg[\sum_{j=1}^{M}\sum_{\ell=1}^{L}\Big\{(1-E_{q(A,W)}[A_{ij}(t)])\Big[E_{q(A,W)}[W_{j\ell}(t)]X_{ij}(t)\log(\Lambda_{q\ell}) + \\
&- E_{q(A,W)}[W_{j\ell}(t)]\Lambda_{q\ell}\Big]\Big\} + \log(\alpha_q(t))\Bigg] + \text{const}.
\end{aligned}$$

We can then recognize the functional form of the multinomial distribution. Thus, we can write:

$$\log q^*(Z|\theta) = \sum_i\sum_t\sum_q Z_{iq}(t)\log r_{iq(t)} + const. \tag{18}$$

Taking the exponential on the two sides, we obtain:

$$q(Z_i) = \prod_{t=1}^{T}\prod_{q=1}^{Q} r_{iq}(t)^{Z_{iq}(t)},$$

where $r_{iq}(t)$ is denoted by:

$$r_{iq}(t) \propto \exp\left(\sum_{j=1}^{M}\sum_{\ell=1}^{L}\left\{(1-E_{q(A,W)}[A_{ij}(t)])\Big[E_{q(A,W)}[W_{j\ell}(t)]X_{ij}(t)\log(\Lambda_{q\ell})+\right.\right.$$
$$\left.\left.-E_{q(A,W)}[W_{j\ell}(t)]\Lambda_{q\ell}\Big]\right\}+\log(\alpha_q(t))\right).$$

However, this distribution needs to be normalized because the matrix $Z(t)$ is a binary matrix and the elements sum to 1 over the values of Q. We can then obtain:

$$q(Z_i)=\prod_{t=1}^{T}\prod_{q=1}^{Q}\tau_{iq}(t)^{Z_{iq}(t)},$$

where

$$\tau_{iq}(t)=\frac{r_{iq}(t)}{\sum_{q_0=1}^{Q}r_{iq_0}(t)}$$

C Derivation of the lower bound

Starting from Eq. 6 we obtain the final expression of the variational lower bound $\mathcal{L}(q,\theta)$ by developing the expression:

$$\begin{aligned}
\mathcal{L}(q,\theta) &= \sum_{A,Z,W} q(A,Z,W)\log\frac{p(X|A,Z,W,\Lambda)p(A\mid\pi)p(Z|\alpha)p(W|\beta)}{q(A,Z,W)}\\
&= E_{q(A,Z,W)}\left[\log\frac{p(X|A,Z,W,\Lambda)p(A\mid\pi)p(Z|\alpha)p(W|\beta)}{\prod_{i=1}^{N}\prod_{j=1}^{M}\prod_{t=1}^{T}q(A_{ij}(t))\prod_{i=1}^{N}\prod_{t=1}^{T}q(Z_i(t))\prod_{j=1}^{M}\prod_{t=1}^{T}q(W_j(t))}\right]\\
&= E_{q(A,Z,W)}[\log p(X|A,Z,W,\Lambda)]+E_{q(A)}[\log p(A\mid\pi)]+E_{q(Z)}[\log p(Z|\alpha)]+\\
&+E_{q(W)}[\log p(W|\beta))]-E_{q(Z)}[\log\prod_{i}q(Z_i)]+\\
&-E_{q(W)}[\log\prod_{j}q(W_j)]-E_{q(A)}[\log\prod_{i}\prod_{j}q(A_{ij})].
\end{aligned}$$

Then we substitute the results obtained in the VE-Step, denoting $E_{q(A,Z,W)}[A_{ij}(t)]=\delta_{ij}(t)$, $E_{q(A,Z,W)}[Z_{iq}(t)]=\tau_{iq}(t)$ and $E_{q(A,Z,W)}[W_{j\ell}(t)]=\eta_{j\ell}(t)$, in order to obtain the final expres-

sion of the lower bound that can be written as follows:

$$\mathcal{L}(q,\theta) = \sum_{t=1}^{T}\sum_{i=1}^{N}\sum_{j=1}^{M}\Bigg\{\delta_{ij}(t)\log(\pi(t)\mathbf{1}_{\{X_{ij}(t)=0\}}) + (1-\delta_{ij}(t))\Bigg[\log(1-\pi(t)) + \\ + \sum_{q=1}^{Q}\sum_{\ell=1}^{L}\Big\{\tau_{iq}(t)\eta_{j\ell}(t)X_{ij}(t)\log\Lambda_{q\ell} - \tau_{iq}(t)\eta_{j\ell}(t)\Lambda_{q\ell}\Big\}\Bigg] + \\ - (1-\delta_{ij}(t))\log(X_{ij}(t)!)\Bigg\} + \sum_{t=1}^{T}\sum_{i=1}^{N}\sum_{q=1}^{Q}\tau_{iq}(t)\log(\alpha_q(t)) + \\ + \sum_{t=1}^{T}\sum_{j=1}^{M}\sum_{\ell=1}^{L}\eta_{j\ell}(t)\log(\beta_\ell(t)) - \sum_{t=1}^{T}\sum_{i=1}^{N}\sum_{q=1}^{Q}\tau_{iq}(t)\log\tau_{iq}(t) + \\ - \sum_{t=1}^{T}\sum_{j=1}^{M}\sum_{\ell=1}^{L}\eta_{j\ell}(t)\log(\eta_{j\ell}(t)) - \sum_{t=1}^{T}\sum_{i=1}^{N}\sum_{j=1}^{M}\Big(\delta_{ij}(t)\log(\delta_{ij}(t)) + (1-\delta_{ij}(t))\log(1-\delta_{ij}(t))\Big).$$

D Proof: Update of Λ

To find the optimal update expression of Λ we compute the derivative of the lower bound $\mathcal{L}(q,\theta)$ in Eq. 16 with respect to Λ and set it equal to zero, as follows:

$$\frac{\partial\log\mathcal{L}(q,\theta)}{\partial\Lambda_{q\ell}} = \sum_{i=1}^{N}\sum_{j=1}^{M}\sum_{t=1}^{T}(1-\delta_{ij}(t))\Big[\frac{\tau_{iq}(t)\eta_{j\ell}(t)X_{ij}(t)}{\Lambda_{q\ell}} - \tau_{iq}(t)\eta_{j\ell}(t)\Big]$$

$$\sum_{i=1}^{N}\sum_{j=1}^{M}\sum_{t=1}^{T}(1-\delta_{ij}(t))\Big[\tau_{iq}(t)\eta_{j\ell}(t)X_{ij}(t) - \tau_{iq}(t)\eta_{j\ell}(t)\Lambda_{q\ell}\Big] = 0$$

$$\sum_{i=1}^{N}\sum_{j=1}^{M}\sum_{t=1}^{T}(1-\delta_{ij}(t))\tau_{iq}(t)\eta_{j\ell}(t)\Lambda_{q\ell} = \sum_{i=1}^{N}\sum_{j=1}^{M}\sum_{t=1}^{T}\tau_{iq}(t)\eta_{j\ell}(t)\Big[X_{ij}(t) - X_{ij}(t)\delta_{ij}(t)\Big]$$

$$\hat{\Lambda}_{q\ell} = \frac{\sum_{i=1}^{N}\sum_{j=1}^{M}\sum_{t=1}^{T}\tau_{iq}(t)\eta_{j\ell}(t)\Big(X_{ij}(t) - \delta_{ij}(t)X_{ij}(t)\Big)}{\sum_{i=1}^{N}\sum_{j=1}^{M}\sum_{t=1}^{T}\tau_{iq}(t)\eta_{j\ell}(t)\Big(1-\delta_{ij}(t)\Big)}$$

E Algorithms

The inference procedure is summarized in Algorithm 1, while the initialization and model selection procedure is summarized in Algorithm 2.

Algorithm 1 VEM-SGD Algorithm (for the Zero-Inflated Poisson distribution)

Require: $X, Q, L, max.iter$, $\alpha, \beta, \pi, \Lambda$ from Initialization.

Initialization of $\tau(t)$ and $\eta(t)$: sampling from $\mathcal{M}(\alpha(t))$ and $\mathcal{M}(\beta(t))$, respectively;

Initialization of $\delta(t)$: matrix of 1, then setting $\delta(t) = 0$ when $X > 0$;

for it = 1 to $max.iter$ **do**

VE-Step:

for p = 1 to p_max **do**

for t = 1 to T **do**

Update $\delta(t)$, $\tau(t)$, $\eta(t)$ **for all** $i = 1, \ldots, N; j = 1, \ldots, M$:

$$\delta_{ij}(t) = \frac{\exp(R_{ij}(t))}{(1 + \exp(R_{ij}(t)))},$$

where:

$$R_{ij}(t) = \log(\pi(t)\mathbf{1}_{\{X_{ij}(t)=0\}}) + \sum_{q=1}^{Q}\sum_{\ell=1}^{L}\Big[- \tau_{iq}(t)\eta_{j\ell}(t)X_{ij}(t)\log\Lambda_{q\ell} + \tau_{iq}(t)\eta_{j\ell}(t)\Lambda_{q\ell}\Big] + \log X_{ij}(t)! - \log(1-\pi(t)).$$

$$\tau_{iq}(t) = \frac{1}{D_q}\exp\left(\sum_{j=1}^{M}\sum_{\ell=1}^{L}\Big\{(1-\delta_{ij}(t))\Big[\eta_{j\ell}(t)X_{ij}(t)\log(\Lambda_{q\ell}) - \eta_{j\ell}(t)\Lambda_{q\ell}\Big]\Big\} + \log(\alpha_q(t))\right).$$

$$\eta_{j\ell}(t) = \frac{1}{D_\ell}\exp\left(\sum_{i=1}^{N}\sum_{q=1}^{Q}\Big\{(1-\delta_{ij}(t))\Big[\tau_{iq}(t)X_{ij}(t)\log(\Lambda_{q\ell}) - \tau_{iq}(t)\Lambda_{q\ell}\Big]\Big\} + \log(\beta_\ell(t))\right).$$

with D_q and D_ℓ normalizing constants.

end for

end for

M-Step:

Update $\theta = (\Lambda, \pi, \alpha, \beta)$.

$\hat{\Lambda}_{q\ell} = \frac{\sum_{i,j,t}\Big\{\tau_{iq}(t)\eta_{j\ell}(t)\Big(X_{ij}(t) - \delta_{ij}(t)X_{ij}(t)\Big)\Big\}}{\sum_{i,j,t}\Big\{\tau_{iq}(t)\eta_{j\ell}(t)\Big(1-\delta_{ij}(t)\Big)\Big\}}$.

for epoch = 1 to Epochs **do**

Update $\hat{\alpha}, \hat{\beta}, \hat{\pi}$:

Loss Evaluation;

Algorithm backpropagation;

Numerical optimization with SGD.

end for

end for

Algorithm 2 Initialization Algorithm

Step 1: Static model selection

Require: $X, Q_{min}, Q_{max}, L_{min}, L_{max}, max\_iter$, $n.sim$.

for Q =Q_{min}, to Q=Q_{max} **do**

for L =L_{min}, to L=L_{max} **do**

Initialize randomly $\alpha, \beta, \pi, \Lambda$;

Run a static version of Zip-dLBM(Q, L) on $t = 1$, computing the ICL;

end for

end for

Obtain Q^* and L^* that gives the highest ICL value.

Step 2: Cascade Process

Require: X , Q^*, L^*, max_iter.

for t = 1 to T **do**

if t =1 **then**

Initialize randomly $\alpha(t = 1), \beta(t = 1), \pi(t = 1)$, Λ;

Run a static version of Zip-dLBM(Q^*, L^*) on $t = 1$;

Store the results $\alpha(t = 1), \beta(t = 1), \pi(t = 1), \Lambda$.

else

Initialize $\alpha(t - 1), \beta(t - 1), \pi(t - 1), \Lambda$;

Run a static version of Zip-dLBM(Q^*, L^*) on t;

Store the results $\alpha(t), \beta(t), \pi(t), \Lambda$.

end if

end for

F Algorithmic Consideration

In this section, we provide detailed technical specifications of the neural networks used in the M-Step of the inference algorithm. We employed fully connected neural networks with two hidden layers, each consisting of 200 neurons. The choice of two hidden layers allows for capturing complex patterns and relationships within the data. We did not used mini-batch training, opting for a full-batch approach where the entire training dataset was used in each iteration. In co-clustering, the clusters formed by rows and columns are interconnected. Any updates made to a subset of rows may impact the clustering of the corresponding columns and vice versa. This interdependency makes it challenging to update mini-batches independently, as changes in one batch may affect the quality and coherence of the clustering solution. Within the VEM algorithm, each iteration involved the optimization of the lower bound. For this purpose, we performed 2000 epochs, where an epoch represents a complete pass through the entire dataset. It is worth noting that our results have demonstrated robustness to the choices we made regarding the size of the neural network. Our experiments and evaluations have shown that the approach remains effective and yields reliable results across a range of network sizes. All the experiments in Section 4 run on CPU on a MacBook Pro, 2020, with a processor of 2,3 GHz Quad-Core Intel Core i7 and 16 GB of RAM

G Other experiment on simulated data

In this section, we present two experiments conducted on simulated data. The first experiment constitutes a benchmark study in which we compare the performance of our model with other state-of-the-art methods. In the second experiment, we simulate datasets that deviate from the assumptions of the original model. This enables us to assess the robustness of our model's assumptions and evaluate its performance under varying scenarios.

G.1 Benchmark study

The goal of this experiment is to compare Zip-dLBM with two state-of-the-art methods to recover the data structure. First, Zip-dLBM is compared with a model based on the same assumptions but which does not take into account the sparsity modeling over time. Denoted by Zip-dLBM$_{\pi(\cdot)=0}$, the model does not take into account the excess of zeros in the data and it is obtained by setting the sparsity parameter $\pi(t)$, with t in $[0, T]$, equal to zero. The other model Zip-dLBM is compared with is dLBM proposed by Marchello et al. (2022) where not only the sparsity is not taken into account but the cluster memberships Z and W are not time-dependent, i.e. cluster switches are not allowed. However, the expected number of interactions between co-clusters (the parameter Λ) changes in time in dLBM.
We also included in the comparison two models that do not consider the dynamic aspect: LBM (Robert et al., 2021b), baseline for model-based co-clustering methods, and k-means (MacQueen, 1967), applied on rows and columns separately. Since the two models do not consider the time aspect, they have been applied at each time instant separately. We chose to evaluate the results with the CARI index. In order to consider the dynamic aspects of the dataset and account for possible switched cluster labels across consecutive time instants, we store the row and column cluster membership results in a unified vector that includes all clustering outcomes over time. This results in vectors with sizes of $N \cdot T$ for row memberships and $M \cdot T$ for column memberships, where N and M represent the number of rows and columns, respectively, and T denotes the total number of time instants. In particular, in order to compare the affectations to the clusters over time, the cluster labels in dLBM were repeated as many times as the number of time instants, and then compared to the affectations of the simulated data using the CARI index. To make this comparison more complete, we defined two simulation scenarios. In Scenario A, the data are simulated as described in Section 4.1 but with a constant sparsity level of 80%, fixed in time. In Scenario B the sparsity evolves in time from 80% to 90% . Table 4 displays the results of this comparison, in terms of average CARI values, reported with standard deviations.
In Scenario A, Zip-dLBM performs well reaching a CARI value of 0.93, on the other hand Zip-dLBM$_{\pi(\cdot)=0}$ suffers from the excessive number of zeros, whose treatment is not con-

sidered, probably affecting the clustering performance. Even worse for dLBM, LBM and kmeans whose CARI index is around 0. For dLBM this is certainly due to the fact that the two latent clustering variables, Z and W, do not evolve over time. LBM and k-means are penalized by the switching clustering labels across different time instants since they are applied independently at each time instant.

In scenario B, Zip-dLBM performs comparably with the previous scenario, with an average CARI index of 0.94 and a smaller standard deviation. Thus, we see that an increasing level of sparsity does not degrade the performance of the model since it is able to distinguish structural zeros from those coming from the Poisson process. This could even help in improving clustering performance. On the contrary, Zip-dLBM$_{\pi(\cdot)=0}$ performs worse than the results obtained in the scenario A probably due to the increased sparsity in the data.

	Zip-dLBM	Zip-dLBM$_{\pi(\cdot)=0}$	dLBM	kmeans	LBM
Scenario A	0.93 ± 0.13	0.27 ± 0.1	0 ± 0	0.01 ± 0	0.01 ± 0.1
Scenario B	0.94 ± 0.03	0.16 ± 0.11	0 ± 0.01	0 ± 0	0.01 ± 0.1

Table 4: Co-clustering results for Zip-dLBM, Zip-dLBM$_{\pi(\cdot)=0}$, dLBM, LBM and kmeans on 50 simulated data according to the two scenarios. Average CARI values are reported with standard deviations.

G.2 Robustness to model assumptions

The goal of this experiment on simulated data is to test the performance of Zip-dLBM when data are not simulated according to the model assumptions. Specifically, we decided to simulate the data from a Zero-Inflated negative binomial distribution. The negative binomial distribution is a discrete probability distribution that models the number of successes in a series of iid Bernoulli trials before a given number of failures, r. Following the notation of Section 2, being a mixture between the negative binomial distribution and a Dirac mass at zero, the Zero-Inflated negative binomial distribution can be formally written

as:

$$\begin{cases} X_{ij}(t)|Z_i(t), W_j(t) = 0 & \text{with probability } \pi(t) \\ X_{ij}(t)|Z_i(t), W_j(t) \sim \mathcal{NB}(X_{ij}(t); r, p) & \text{with probability } 1 - \pi(t). \end{cases}$$

The probability mass function of the negative binomial is given by:

$$f(k, r, p) = \binom{k + r - 1}{k} \cdot (1 - p)^r \cdot p^k = \frac{\Gamma(k + r)}{k!\Gamma(r)}(1 - p)^r p^k,$$

where k is the number of successes and p is the probability of success. When modeling counts data the negative binomial distribution is often a valid alternative to the Poisson one, because it allows the mean and the variance to be different: Mean: $\lambda = \dfrac{pr}{1-p}$; Variance: $= \dfrac{pr}{(1-p)^2} = \lambda + \frac{1}{r}\lambda^2$. A particular property of the negative binomial distribution is that it converges to the Poisson distribution, with expected value Λ, when $r \to \infty$.

To accurately evaluate the performance of Zip-dLBM we simulate with the negative

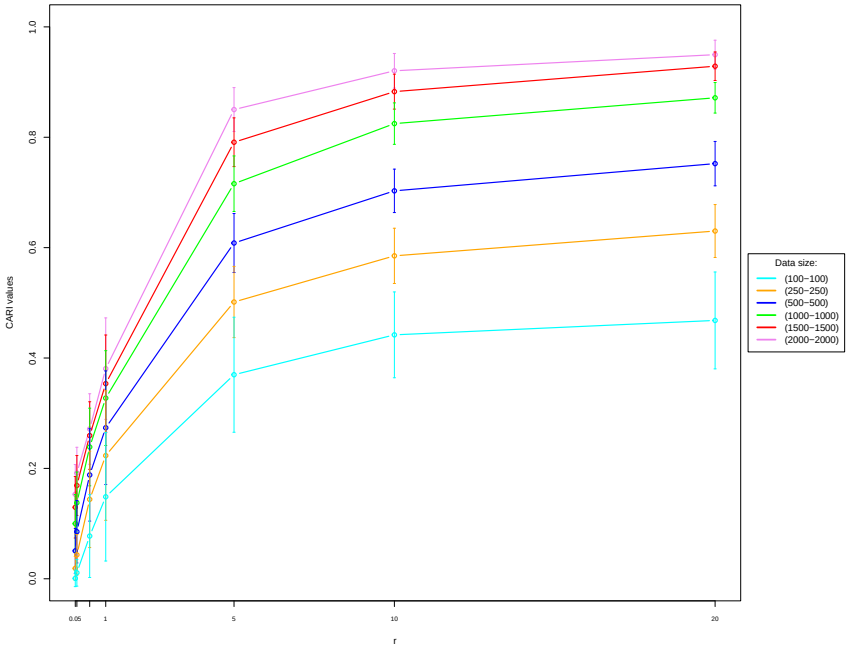

Figure 14: Evolution of the CARI (on the y-axis) according to r (on the x-axis), where each line represent a different data size.

binomial distribution data sets for each value of r equal to 0.05, 0.1, 0.5, 1, 5, 10, 20, while keeping the values of Λ unchanged to the ones of the introductory example in Section

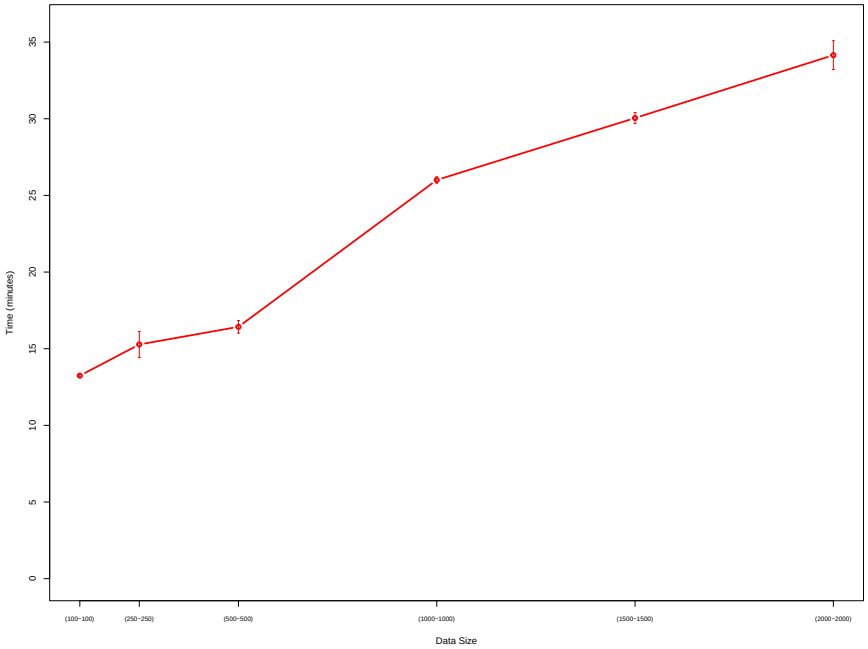

Figure 15: Evolution of the average running time (on the y-axis), displayed with the standard deviation, according to different data sizes (on the x-axis).

4.1. Also, to evaluate the robustness of the model to data size we simulate data sets with different size for each value of r. The datasets have been simulated with (row-column) size 100-100, 250-250, 500-500, 1000-1000, 1500-1500, 2000-2000, respectively. Figure 14, reports the results of the experiment, depicting the evolution of the values taken by the CARI index (on the y-axis) across different values of the parameter r (on the x-axis) and for different data sizes. Looking at these results we can observe that for values of r very close to zero, all models have difficulties in identifying the correct cluster partition. However, as r increases, models with larger data sizes achieve an average CARI value close to 1, indicating improved clustering performance. Also, we see The method becomes increasingly robust as the data size increases. In the same experiment, we also evaluate the average running time for each simulated dataset across different r values. Figure 15 presents these results, with the x-axis representing the data size and the y-axis indicating the running time in minutes. Each point on the graph corresponds to the average running time, accompanied by its standard deviation. Notably, we observe that the running time demonstrates a relatively

linear relationship with the data size, suggesting scalability of the algorithm.

References

Ailem, M., Role, F., and Nadif, M. (2017). Sparse poisson latent block model for document clustering. *IEEE Transactions on Knowledge and Data Engineering*, 29(7):1563–1576.

Banerjee, A., Dhillon, I., Ghosh, J., and Modha, D. (2007). A generalized maximum entropy approach to bregman co-clustering and matrix approximation. *Journal of Machine Learning Research*, 8:8 pages 1919–1986.

Bergé, L. R., Bouveyron, C., Corneli, M., and Latouche, P. (2019). The latent topic block model for the co-clustering of textual interaction data. *Computational Statistics & Data Analysis*, 137:247–270.

Biernacki, C., Celeux, G., and Govaert, G. (2000). Assessing a mixture model for clustering with the integrated completed likelihood. *IEEE transactions on pattern analysis and machine intelligence*, 22(7):719–725.

Bishop, C. M. (2006). Approximate inference. pages 461–517. Springer-Verlag, Berlin, Heidelberg.

Boutalbi, R., Labiod, L., and Nadif, M. (2020). Tensor latent block model for co-clustering. *International Journal of Data Science and Analytics*, pages 1–15.

Boutalbi, R., Labiod, L., and Nadif, M. (2021). Implicit consensus clustering from multiple graphs. *Data Mining and Knowledge Discovery*, 35(6):2313–2340.

Bouveyron, C., Bozzi, L., Jacques, J., and Jollois, F.-X. (2018). The functional latent block model for the co-clustering of electricity consumption curves. *Journal of the Royal Statistical Society: Series C (Applied Statistics)*, 67(4):897–915.

Bouveyron, C., Celeux, G., Murphy, T. B., and Raftery, A. E. (2019). *Model-based clustering and classification for data science: with applications in R*, volume 50. Cambridge University Press.

Casa, A., Bouveyron, C., Erosheva, E., and Menardi, G. (2021). Co-clustering of time-dependent data via the shape invariant model. *Journal of Classification*, 38(3):626–649.

Corneli, M., Bouveyron, C., and Latouche, P. (2020). Co-clustering of ordinal data via latent continuous random variables and not missing at random entries. *Journal of Computational and Graphical Statistics*, pages 1–15.

Dempster, A. P., Laird, N. M., and Rubin, D. B. (1977). Maximum likelihood from incomplete data via the em algorithm. *Journal of the Royal Statistical Society: Series B (Methodological)*, 39(1):1–22.

Dhillon, I. S. (2001). Co-clustering documents and words using bipartite spectral graph partitioning. In *Proceedings of the seventh ACM SIGKDD international conference on Knowledge discovery and data mining*, pages 269–274.

Dhillon, I. S., Mallela, S., and Modha, D. S. (2003). Information-theoretic co-clustering. In *Proceedings of the ninth ACM SIGKDD international conference on Knowledge discovery and data mining*, pages 89–98.

Ding, C., Li, T., Peng, W., and Park, H. (2006). Orthogonal nonnegative matrix t-factorizations for clustering. In *Proceedings of the 12th ACM SIGKDD international conference on Knowledge discovery and data mining*, pages 126–135.

Fenn, D. J., Porter, M. A., Mucha, P. J., McDonald, M., Williams, S., Johnson, N. F., and Jones, N. S. (2012). Dynamical clustering of exchange rates. *Quantitative Finance*, 12(10):1493–1520.

Forbes, F., Arnaud, A., Lemasson, B., and Barbier, E. (2019). Component elimination strategies to fit mixtures of multiple scale distributions. In *Statistics and Data Science: Research School on Statistics and Data Science, RSSDS 2019, Melbourne, VIC, Australia, July 24–26, 2019, Proceedings 1*, pages 81–95. Springer.

Gallaugher, M. P., Biernacki, C., and Mcnicholas, P. D. (2022). Parameter-wise co-clustering for high-dimensional data. *Computational Statistics*, pages 1–23.

Gent, C. and Sheppard, C. (1992). Special feature. predicting time series by a fully connected neural network trained by back propagation. *Computing & Control Engineering Journal*, 3(3):109–112.

Govaert, G. and Nadif, M. (2003). Clustering with block mixture models. *Pattern Recognition*, 36(2):463–473.

Govaert, G. and Nadif, M. (2008). Block clustering with bernoulli mixture models: Comparison of different approaches. *Computational Statistics & Data Analysis*, 52(6):3233–3245.

Govaert, G. and Nadif, M. (2010). Latent block model for contingency table. *Communications in Statistics - Theory and Methods*, 39(3):416–425.

Jaakkola, T. S. and Jordan, M. I. (1997). A variational approach to bayesian logistic regression models and their extensions. In *Sixth International Workshop on Artificial Intelligence and Statistics*, pages 283–294. PMLR.

Jacques, J. and Biernacki, C. (2018). Model-based co-clustering for ordinal data. *Computational Statistics & Data Analysis*, 123:101–115.

Jordan, M. I., Ghahramani, Z., Jaakkola, T. S., and Saul, L. K. (1998). An introduction to variational methods for graphical models. In *Learning in graphical models*, pages 105–161. Springer.

Keribin, C., Brault, V., Celeux, G., and Govaert, G. (2015). Estimation and selection for the latent block model on categorical data. *Statistics and Computing*, 25(6):1201–1216.

Kingma, D. P. and Ba, J. (2014). Adam: A method for stochastic optimization. *arXiv preprint arXiv:1412.6980*.

Labiod, L. and Nadif, M. (2011). Co-clustering under nonnegative matrix tri-factorization. In *International Conference on Neural Information Processing*, pages 709–717. Springer.

Lambert, D. (1992). Zero-inflated poisson regression, with an application to defects in manufacturing. *Technometrics*, 34(1):1–14.

Li, N., Elashoff, D. A., Robbins, W. A., and Xun, L. (2011). A hierarchical zero-inflated log-normal model for skewed responses. *Statistical Methods in Medical Research*, 20(3):175–189.

Liang, D., Corneli, M., Bouveyron, C., and Latouche, P. (2021). Deepltrs: A deep latent recommender system based on user ratings and reviews. *Pattern Recognition Letters*, 152:267–274.

Lindstrom, M. J. (1995). Self-modelling with random shift and scale parameters and a free-knot spline shape function. *Statistics in medicine*, 14(18):2009–2021.

Lomet, A. (2012). *Sélection de modèle pour la classification croisée de données continues*. PhD thesis, Compiègne.

Lu, Z., Wang, S., Liu, G., and Nie, F. (2023). Robust weighted co-clustering with global and local discrimination. *Pattern Recognition*, 138:109405.

MacQueen, J. (1967). Classification and analysis of multivariate observations. In *5th Berkeley Symp. Math. Statist. Probability*, pages 281–297. University of California Los Angeles LA USA.

Malsiner-Walli, G., Frühwirth-Schnatter, S., and Grün, B. (2016). Model-based clustering based on sparse finite gaussian mixtures. *Statistics and computing*, 26(1-2):303–324.

Marchello, G., Fresse, A., Corneli, M., and Bouveyron, C. (2022). Co-clustering of evolving count matrices with the dynamic latent block model: application to pharmacovigilance. *Statistics and Computing*, 32(3):1–22.

Matias, C. and Miele, V. (2017). Statistical clustering of temporal networks through a dynamic stochastic block model. *Journal of the Royal Statistical Society: Series B (Statistical Methodology)*, 79(4):1119–1141.

Nowicki, K. and Snijders, T. A. B. (2001). Estimation and prediction for stochastic blockstructures. *Journal of the American statistical association*, 96(455):1077–1087.

Ospina, R. and Ferrari, S. L. (2012). A general class of zero-or-one inflated beta regression models. *Computational Statistics & Data Analysis*, 56(6):1609–1623.

Paszke, A., Gross, S., Chintala, S., Chanan, G., Yang, E., DeVito, Z., Lin, Z., Desmaison, A., Antiga, L., and Lerer, A. (2017). Automatic differentiation in pytorch.

Rand, W. M. (1971). Objective criteria for the evaluation of clustering methods. *Journal of the American Statistical Association*, 66(336):846–850.

Ridout, M., Hinde, J., and Demétrio, C. G. (2001). A score test for testing a zero-inflated poisson regression model against zero-inflated negative binomial alternatives. *Biometrics*, 57(1):219–223.

Robert, V. (2017). Coclustering for the analysis of pharmacovigilance massive datasets. *HAL*, 2017.

Robert, V., Vasseur, Y., and Brault, V. (2021a). Comparing high-dimensional partitions with the Co-clustering Adjusted Rand Index. *Journal of Classification*, 38:158–186.

Robert, V., Vasseur, Y., and Brault, V. (2021b). Comparing high-dimensional partitions with the co-

clustering adjusted rand index. *Journal of Classification*, 38:158–186.

Selosse, M., Jacques, J., and Biernacki, C. (2020). Model-based co-clustering for mixed type data. *Computational Statistics & Data Analysis*, 144:106866.

Yang, T., Chi, Y., Zhu, S., Gong, Y., and Jin, R. (2011). Detecting communities and their evolutions in dynamic social networks—a bayesian approach. *Machine learning*, 82(2):157–189.